This manuscript has been accepted for publication in Icarus

Terrestrial formation of calcium sulfate and carbonate assemblages in Atacama CO chondrites: Implications for Martian evaporitic environments

Gabriel A. Pinto[1,2,5]*, Vinciane Debaille[1], Jolantha Eschrig[2], Alexandre Corgne[3], Kevin Soto[4], Thierry Leduc[5], Sophie Decree[5], Steven Goderis[2]

[1]*Laboratoire G-Time & Brussels Laboratory of the Universe (BLU), Université Libre de Bruxelles, 1050 Brussels, Belgium*

[2]*Archaeology, Environmental Changes, and Geo-Chemistry, Vrije Universiteit Brussel, 1050 Brussels, Belgium*

[3]*Instituto de Ciencias de la Tierra, Universidad Austral de Chile, Valdivia, Chile*

[4]*Departamento de Ciencias Geológicas, Universidad Católica del Norte, Antofagasta, Chile*

[5]*Institute of Natural Sciences, Geological Survey of Belgium, 1000, Brussels, Belgium*

*Corresponding author: gabriel.angel.pinto.morales@ulb.be

Abstract

Evaporites are frequently reported in carbonaceous chondrites from hot and cold deserts, yet their origin remains debated between formation on the parent body or by post-fall terrestrial alteration. Here, we present a systematic characterization of Ca sulfate and Ca carbonate assemblages in four CO carbonaceous chondrites from different dense collection areas of the Atacama Desert (Los Vientos 123, El Médano 464, Calama 031, Paposo 088). We combine backscattered electron imaging, EDS, X-ray compositional mapping, Raman spectroscopy, and modal point counting to assess the distribution, mineralogy, and formation context of evaporites. Evaporites occur mainly as pore- and vein-filling phases and as replacements of Fe sulfides. Los Vientos 123 and El Médano 464 contain high abundances of Ca sulfates (~2.5 ± 0.35 vol%), Calama 031 is dominated by Ca carbonate veins (1.4 ± 0.26 vol%) with minor Ca sulfate, and Paposo 088 shows only low Ca sulfate contents (0.47 ± 0.15 vol%). These phases are systematically associated with Fe oxyhydroxides, jarosite-like phases, and strongly altered sulfides. The sulfate- and carbonate-rich assemblages in CO chondrites correlate with local soil geochemistry and microclimates. Limestone bedrock and more rain-influenced inland set different evaporite assemblages compared to coastal areas characterized by marine aerosols and salt-rich soils. Raman spectra indicate that the dominant Ca sulfate polymorph is anhydrite, lacking OH-stretching bands, consistent with precipitation from low-water activity, chloride-nitrate-rich

brines and limited subsequent hydration. Disordered carbonaceous matter locally sheltered within sulfate-rich areas suggests that secondary evaporites can trap and preserve organic material, even if non-biological. Our results thus support (i) a terrestrial origin for Ca sulfates and Ca carbonates in Atacama CO chondrites; (ii) the stability of anhydrite as an indicator of extremely low water activity; and (iii) process analogues for evaporite formation in Martian settings, where anhydrite regions may be key targets to reconstruct aqueous conditions and assess organic preservation on Mars.

Keywords: Carbonaceous chondrites, Evaporites, Sulfates, Carbonates, Atacama Desert, Weathering of meteorites, Mars, Martian analogue

1- Introduction

Chondrites are fragments of asteroids that escaped differentiation and therefore preserved relict components formed during the first few million years of the Solar System. Among the various chondrite classes, Ornans-like carbonaceous (CO) chondrites are some of the most primitive samples experiencing only low-grade thermal metamorphism (peak ≤ 600 °C; Huss et al., 2006; Bonal et al., 2006) and limited aqueous alteration (Alexander et al., 2018; Doyle et al., 2015; Marrocchi et al., 2018). With very few exceptions (i.e., MIL 07687; Haenecour et al., 2020; Prestgard et al., 2021), all COs range from petrologic grade 3.0 to 3.8 (Scott and Jones, 1990; Chizmadia et al., 2002). Their fine-grained matrices host insoluble and soluble organic matter as well as presolar grains (e.g., Bonal et al., 2006; Nittler et al., 2018; Haenecour et al., 2018), which makes them especially appropriate for the study of nebular processes. However, as residence on Earth can modify primary phases, a good understanding of terrestrial weathering processes across different environments is essential to assess such nebular processes and allow for the identification of the least altered COs.

Meteorites are preferentially preserved in hot and cold deserts, where the environment favors slow chemical weathering leading to terrestrial ages of hundreds of thousands up to millions of years (Nishiizumi et al., 1989; Bland et al., 2006; Drouard et al., 2019). Nonetheless, even in these dry environments, limited but repeated moisture fluxes promote (i) oxidation/hydroxylation of metals and sulfides, (ii) partial replacement of silicates by clays/oxides, and (iii) precipitation of terrestrial evaporites in pores and fractures (Wlotzka, 1993; Lee and Bland, 2004; Abreu and Brearley, 2005; Velbel, 2014). Furthermore, organic contaminants may also accumulate through the influence of microorganisms, mosses, lichens, algae, soils, and anthropogenic residues from the fall site (e.g., Benzerara et al., 2007; Sephton, 2002; Tait et al., 2022; Pinto et al., 2025). Weathering degrees are generally assigned to individual samples based on oxidation products (Wlotzka, 1993; Bland et al., 2006), yet several studies highlight the diagnostic value of salts (Velbel, 1988; Zurfluh et al., 2016). For instance, Antarctic meteorites with terrestrial evaporites are designated with the letter "e" (Lindstrom, 1989; Velbel, 2014), whereas hot desert finds generally are not, potentially biasing interpretations of chemical composition, isotopic signatures, and organic abundances.

Terrestrial evaporites in meteorites (e.g., carbonates, sulfates, halides) form when liquid water, derived from rain or atmospheric moisture, interacts with the rock and then evaporates or freezes, which produces supersaturated brines from which these minerals precipitate (Velbel, 1988; Lee and Bland, 2004; Losiak and Velbel, 2011). Their sequence typically follows decreasing solubility with carbonates forming first, followed by Ca sulfates, and finally chlorides (Bland et al., 2006; Zurfluh et al., 2013). Evaporitic minerals are more frequently detected in carbonaceous chondrites compared to ordinary chondrites, and more often in petrologic type 3 relative to higher petrologic types (Velbel, 1988; Losiak and Velbel, 2011). Chondrites can continue to interact with the atmosphere even after they were

collected, potentially forming Ca sulfates post-recovery (Velbel, 2014; Gounelle and Zolensky, 2001), which are among the most common evaporitic products in meteorites (Losiak and Velbel, 2011; Bland et al., 2006; Lee et al., 2021). Among them, the $CaSO_4$-H_2O system, including gypsum ($CaSO_4 \cdot 2H_2O$), bassanite ($CaSO_4 \cdot 0.5H_2O$), and anhydrite ($CaSO_4$), with additional anhydrite polymorphs along the hydration-dehydration pathway (Sarma et al., 1998; Prieto-Taboada et al., 2014; Van Driessche et al., 2019). These polymorphs have distinct SO_4 bending/stretching and OH stretching bands in hydrated phases, enabling their unambiguous identification. Raman spectroscopy is also used to constrain the Fe oxyhydroxide phases and state of polyaromatic carbon via the D (~1350 cm^{-1}) and G (~1580 cm^{-1}) bands. The positions, widths, and intensity ratios of these bands track graphitization and metamorphic grade (Bonal et al., 2006; Busemann et al., 2007). This makes Raman spectroscopy an ideal method for assessing intrinsic chondritic material and terrestrial weathering phases.

Meteorites recovered from the Atacama Desert generally show better preservation than those from other hot deserts (Pinto et al., 2024b; Sadaka et al., 2025; Hutzler et al., 2016). The Atacama Desert shows three main morphotectonic provinces (**Fig. 1**). The Coastal Range (CR), located adjacent to the Pacific Ocean on a Cretaceous volcanic and intrusive basement, extends in a north-south direction and reaches elevations up to 2000 m above sea level (masl). This area is regularly influenced by coastal fog (i.e., the marine stratocumulus cloud bank *camanchaca* that moves inland) generated through radiation, advection, and orographic processes (Goudie et al., 2002; Lobos-Roco et al., 2024). East of the CR is the Central Depression (CD), a basin filled with Neogene sedimentary sequences, Paleogene volcanic deposits, and extensive Quaternary alluvial fan deposits (Riquelme et al., 2007; Hartley and Chong, 2002). The CD is largely shielded from moisture by the CR to the west and the Andes Mountain Belt to the east. Nonetheless, moisture can reach certain areas of the

CD, depending on local topography and the condensation of water through orographic processes (Lobos-Roco et al., 2024). The Calama dense collection area (DCA), situated in the Pre-Andean Range-Basement (PRB; Pinto et al., 2024b), comprises several Quaternary and Neogene volcanic sequences and extended basements filled by Neogene sedimentary sequences (Riquelme et al., 2007). The Calama Basin is an elongated terrestrial forearc basin located between the Western Cordillera of the Andes, which form the eastern margin, and the Cordillera Domeyko or Pre cordillera Highlands that forms the western margin (de Wet et al., 2015).

CO chondrites are generally overrepresented among carbonaceous chondrites in the Atacama Desert collections relative to the global meteorite inventory (60.9±14.1% and 24.3±1.5 %, respectively; Pinto et al., 2024b), and are commonly filled by Ca sulfates in µm-scale pores and fractures, especially in fine-grained rims (Pinto et al., 2022). This makes the Atacama Desert a perfect environment to study the processes involved in the formation of secondary Ca sulfates in meteorites. One proposed formation process is the interaction of marine-fog moisture along the Pacific coast with the saline soils inland (Valenzuela, 2011; Pourkhorsandi et al., 2017; Pinto et al., 2024b). However, no systematic comparison of evaporite occurrence across the Atacama's DCAs has been done at present.

Such a comparison is relevant not only shine a light on the origin of the weathering processes taking place in the Atacama Desert but also be applicable to other environments like Mars, where jarosite, Ca sulfates, and localized carbonates are widespread and likely formed under similarly oxidizing, water-limited conditions (e.g., Klingelhöfer et al., 2004; Tosca and McLennan, 2009). The Atacama Desert is considered as one of the best terrestrial analogues for Mars due of its long-term hyperaridity, high UV radiation, oxidizing surface conditions, and extremely low organic content (Navarro-González et al., 2003; Azua-Bustos et al., 2022). In addition, Atacama soils accumulate sulfate-, nitrate-, chloride-, and

perchlorate-rich salts under persistent water limitation, making them a useful natural setting for investigating evaporite formation and preservation under Mars-relevant conditions (Voigt et al., 2020; Arens et al., 2021).

Here we test how local climate and geology modulate evaporite formation in CO chondrites from four Atacama DCAs spanning all three morphotectonic provinces. For this, we combine backscattered electron (BSE) imaging, energy-dispersive X-ray spectroscopy (EDS), and micro-Raman analyses to (i) map the occurrence and textures of Ca sulfates and secondary carbonates, (ii) relate them to internal versus external salt inputs, and (iii) discuss implications for evaporite formation in the Atacama Desert and their relevance to Martian sulfate-carbonate assemblages.

2- Materials and Methods

2.1 Samples and preparation

We surveyed evaporitic minerals in four CO carbonaceous chondrites: Los Vientos 123 (LoV 123, CO3.1), El Médano 464 (EM 464, CO3), Calama 031 (CO3), and Paposo 088 (CO3). All samples were collected across different DCAs within the main morphotectonic units of the Atacama Desert (**Fig. 1**). Three in-house thick sections (LoV 123, EM 464, Calama 031) were prepared by methanol-assisted polishing. The Paposo 088 section was previously prepared at the Pelom Kura Repository (Valdivia, Chile), following the repository's standard water-assisted polishing protocol. Because all meteorites used in this work were originally recovered by private collectors (2016-2022; **Table 1**), prior use of water during cutting cannot be ruled out. All sections were cut from the interiors of the main mass, a few millimeters away from the fusion-crust remnants, except for the section of LoV 123

which spans from the fusion-crust remnant to the interior. Sections were stored at room temperature and under dry conditions.

2.2 Scanning Electron Microscopy

The distribution and petrography of the evaporites were investigated by optical microscopy, BSE imaging, and EDS/X-ray compositional mapping. The secondary electron microscopes (SEM) used were (i) a SNE-4500M Plus coupled with a Bruker XFlash® EDS QUANTAX system, operating at 110 µA emission current and 15 kV (Laboratoire G-Time, Brussels, Belgium), (ii) a ZEISS EVO MA10 equipped with an Oxford Instruments X-act detector, operating with a 100 µA beam current at 20 kV (Universidad Austral de Chile, Valdivia, Chile), and (iii) a JEOL IT800 equipped with an Oxford Instruments EDX Ultim Max 100, operating with 50 mA beam current at 23 kV (Institute of Natural Sciences, Brussels, Belgium). The analytical uncertainty of the EDS measurements was estimated from instrumental stability, based on repeated analyses (2-3) of the same phase. Prior to SEM-EDS analysis, the polished sections were coated with 20 nm of carbon.

2.3 Micro-X-Ray Fluorescence

The major and trace element compositions of three CO carbonaceous chondrites (LoV 123, EM 464, and Calama 031) were semi-quantitatively analyzed by energy-dispersive micro-X-ray fluorescence (µ-XRF) scanning at the Department of Analytical-Environmental and Geo-Chemistry (AMGC, VUB, Belgium). Measurements were carried out with an M4 Tornado benchtop µ-XRF surface scanner equipped with XFlash 430 silicon drift detectors. Element maps were collected under low-vacuum conditions (20 mbar) using 50 kV and 600

μA, with a spot size and spatial resolution of 10 μm and an integration time of 3 ms per pixel. This method provides high-resolution elemental distributions as qualitative multi-element maps and semi-quantitative single-element heatmaps in a rapid, non-destructive, and cost-effective mode to investigate flat surfaces (Kaskes et al., 2021). Particular attention was paid for elements affected by peak overlap, such as Co-Kα and Fe-Kβ (6.930 keV), which were resolved using automatic peak deconvolution in the Bruker M4 software (**Fig. S1**).

2.4 Micro-Raman spectroscopy

Evaporite-bearing pores and veins, together with Fe oxyhydroxides, were analyzed using a SENTERRA dispersive Raman microscope (Bruker) at the Institute of Natural Sciences (Brussels). A total of 63, 35, and 33 spot measurements were performed on evaporite domains in LoV 123, EM 464, and Calama 031, respectively. Prior to analysis, the carbon coat applied for SEM-EDS was removed with a 1 μm diamond pad. Then a 532 nm solid-state laser, with a spectral resolution of 3-5 cm^{-1}, and a 50x objective was used. The laser power was set to 5-10 mW for the sulfates (to avoid thermal alteration) and 10-20 mW for the carbonates, with acquisition times of 3-5 s and 3-5 accumulations per spectrum. Spot measurements were replicated within each evaporite domain and compared against natural standards (gypsum from Pellenberg and anhydrite from Kłodawa) to verify phase assignments under the same operating conditions (**Fig. S2**).

Raman spectra of Fe oxyhydroxides were acquired using low laser power to minimize thermal alteration and laser-induced phase transformation during analysis (Hanesch et al., 2009). Analyses were performed at 0.2 mW with an acquisition time of 300 s, 2 accumulations per spectrum, and a 100x objective lens. For potential jarosite-like phases, spectra were collected at the same laser power, with an acquisition time of 60 s, 8-10

accumulations per spectrum, and 50x to 100x objective lenses. Measurements were replicated and compared with natural standards analyzed under the same conditions to verify phase assignments, including magnetite from Arendal (Norway), goethite from Cap Blanc Nez (France), hematite from the Fortuna mine (Germany), jarosite from Sierra Almagrera (Spain) (**Fig. S3**).

Spectra showing first-order D (~1350 cm^{-1}) and G (~1580 cm^{-1}) bands were fit with a custom-developed Python routine. After a linear baseline subtraction between 1100-1800 cm^{-1}, a Lorentzian fit using several Lorentzian profiles (one G component; up to four in the D region; **Fig. S4**) was performed, yielding r^2 values between 0.97 and 0.99. This fitting approach is widely applied in Raman spectral analyses of carbonaceous materials in chondrites (e.g. Bonal et al., 2016; Chan et al., 2017). We report peak positions (ω), full widths at half maximum (FWHM), and the I_D/I_G ratios in **Table 2**.

2.5 Modal abundances and size distribution

Modal abundances of silicate/mesostasis (chondrules and amoeboid olivine aggregates), matrix, CAIs, Fe-Ni alloys, Fe sulfides, Fe oxyhydroxides, sulfates, and carbonates were determined using representative areas of 149.2, 51.7, 10.5, and 6.6 mm^2 for LoV 123, Calama 031, EM 464, and Paposo 088, respectively (**Table 1**). We performed manual point counting (~2000 random points per section) in JMicroVision, using BSE mosaics, EDS/X-ray maps, and optical images (typically 100 to 200x magnification). Counting uncertainties were estimated assuming Poisson statistics following Pinto et al. (2022). Evaporite-bearing pores were traced manually in Fiji/ImageJ (Schindelin et al., 2012) and apparent spherical diameters were calculated from the measured areas as equivalent-circle diameters (see Pinto et al., 2021).

3- Results

3.1 Petrographic characterization of secondary evaporites

Evaporites in the four CO chondrites are primarily Ca sulfates and Ca carbonates. Whole-section µ-XRF maps of EM 464, Calama 031, and LoV 123 reveal clear inter-sample differences in the abundance and distribution of Ca- and S-rich secondary phases (**Fig. 2**). Ca-S enrichments are most extensive in LoV 123, more localized in EM 464, and comparatively rare in Calama 031. LoV 123, Paposo 088, and EM 464 are sulfate-dominated, with Ca sulfate completely or partially filling veins and cavities across all chondritic components (**Figs. 2-3**). Calama 031 is carbonate-dominated, hosting a dense vein network from a few µm to ~30 µm thickness that traverses the entire section (~15 mm; **Fig. 3e,f**). In all COs, weathered Fe sulfides in both matrix and chondrules are associated with Fe oxyhydroxides and Ca sulfate (**Fig. 3b**).

In LoV 123, sulfate veins range from a few µm to 1.5 mm in length and <1-30 µm in width. Narrow veins (<5 µm) track interfaces between matrix and coarse components (chondrules, CAIs, isolated olivine). The X-ray maps show smooth alteration textures accompanied by localized Fe and Ni enrichments. This pattern is especially pronounced in EM 464, where it suggests an alteration front extending from the left to the right side of the section (**Figs. 2, S1**). Thick veins display compositional heterogeneity in Ca at the µm-scale (**Fig. 3d**). Acicular Fe oxyhydroxides occur as needle-like aggregates intergrown with Ca sulfate (**Fig. 3d**) and within Fe sulfides alteration assemblages (**Fig. 3b**). In EM 464, sulfates are mainly present as cavity fills (apparent diameters 3-30 µm; **Fig. 4a**), and many veins are only partially filled (**Fig. 5a**). In both samples, Ca sulfates contain µm-scale voids and locally

preserve polishing scratches. Sulfates in Paposo 088 partially fill some veins and pores. Since most of the infill appears below the sample polished surface, sulfate loss during sample preparation may have occurred (**Fig. 3g,h**).

Although Calama 031 is carbonate-rich, minor amounts of Ca sulfate occur at vein margins, in weathered Fe sulfides, and within CAI/chondrule pores. BSE and X-ray maps reveal incompletely filled carbonate veins with heterogeneity in Ca distribution (**Fig. 3f**). The occurrence of local Cl- and S-rich domains, together with minor Al, Na, and K and embedded chondrule/matrix fragments, is consistent with localized fluid-mediated alteration under restricted fluid circulation (Abreu and Brearley, 2005). Mixed sulfate-carbonate pore fills are rare.

CAIs in all COs host abundant secondary Ca sulfates within intracrystalline pores of Ca-rich mineral phases and along CAI-matrix contacts (**Fig. 3b**). In Calama 031, CAIs also contain coexisting carbonates and Ca sulfates in intra and intercrystalline pores, similar to what is observed in the Cold Bokkeveld chondrite (CM2; Lee, 1993). In the other COs, CAI sulfates occur largely without carbonates. Within chondrules, Ca sulfate occurs (i) in intercrystalline pores within Fe-rich chondrules **(Fig. 3e,f)** and (ii) with weathered sulfides inside metal blebs of Mg-rich chondrules (**Fig. 5d**). Fe sulfide alteration assemblages comprise Ca sulfates, Fe oxyhydroxides, and a Ca-bearing jarosite-like phases (**Fig. 5b**). Raman spectra further show that these Fe oxyhydroxides consist of variable mixtures of hematite- and goethite-like phases, locally associated with sulfate bands (**Fig. S5**). Some areas also show minor Cl- and Ni-enrichments in SEM-EDS analyses. Calcium sulfate margins within Fe sulfides are commonly bordered by acicular goethite, consistent with the Raman spectra (**Fig. S5**; 615-760 cm^{-1}; Hanesch et al., 2009).

Evaporite-bearing veins and pores have sharp interfaces with host lithologies, typically lined by a nanometric Fe oxyhydroxide rim (**Fig. 3h**). Adjacent silicates remain

unaltered, while Fe sulfide and Fe-Ni metal show extensive alteration near sulfates (**Fig. 5**). The degree of Fe sulfide weathering is independent of grain size (**Fig. 4b**), with pristine μm-scale Fe sulfides occurring beside heavily altered sulfides and evaporites. Similarly, Mg-rich chondrules can host pristine metal blebs next to altered Fe-Ni alloys and Fe sulfides (**Fig. 5d**).

3.2 Raman spectra of secondary evaporites

Raman spot and line analyses of secondary Ca sulfates in LoV 123, EM 464, and Calama 031 consistently show SO_4 bands at ~1017 cm^{-1} (ν_1), ~417/500 cm^{-1} (ν_2), ~1128/1158 cm^{-1} (ν_3), and ~628/676 cm^{-1} (ν_4) (**Figs. 6-7**). For some spectra (<5%; N=134) ν_1 is shifted to ~1014-1015 cm^{-1} indicating the presence of Fe oxyhydroxides or sulfides. Although ν_1 ~ 1015 cm^{-1} can indicate bassanite (Prieto-Taboada et al., 2014), our sulfate spectra show a flat >1200 cm^{-1} region and no OH bands at 3400-3500 cm^{-1} (**Fig. 6**). Comparison with reference gypsum (ν_1 ~ 1006 cm^{-1}; single ν_3 ~ 1134 cm^{-1}; OH stretching band) and anhydrite (ν_1 ~ 1017 cm^{-1}; ν_3 doublet; no OH) confirms that analytical conditions did not induce dehydration (**Fig. S2; Fig. 6**). We attribute the small ν_1 downshifts (1-2 cm^{-1}) to lattice impurities rather than hemihydrate, consistent with the absence of structural OH (Prieto-Taboada et al., 2014).

Carbon bands (D, G) are present in 17.1% (EM 464) and 5.7% (LoV 123) of Ca sulfate spectra, occurring along veins, evaporite-bearing pores, CAI/chondrule borders, and near weathered Fe sulfides. No carbon bands were detected in Calama 031. Band positions (ω_D, ω_G), widths ($FWHM_D$, $FWHM_G$), and I_D/I_G ratios (**Table 2**) match disordered carbonaceous matter typical of CO chondrites (I_D/I_G = 0.72 ± 0.01 to 1.58 ± 0.12; Bonal et al., 2016).

Ca sulfate spectra also show olivine doublets at 815-825 and 838-857 cm^{-1} (Kuebler et al., 2006) in 5.7% (EM 464) and 17.4% (LoV 123) of spots, consistent with μm-nm olivine inclusions within evaporites. Peaks at 220-230, 290-300, 385-395, and 545-550 cm^{-1} indicate goethite/hematite (Hanesch et al., 2009). At sulfate-sulfide boundaries, additional bands at 370-390 and 700-720 cm^{-1} point to potential ferrihydrite (Hanesch et al., 2009; Abreu and Brearley, 2005). Raman spectra acquired from weathered Fe sulfide grains are characterized by weak, broad features and locally elevated background (**Fig. S5**), and do not allow unambiguous discrimination between Fe sulfide phases (e.g., troilite and pyrrhotite; Li et al., 2023).

In Calama 031, carbonates measured by SEM-EDS are confirmed by a ν_1 (CO_3^{2-}) band ~1080 cm^{-1} (Cloots, 1991), with supplementary bands near ~710 and ~280 cm^{-1}, characteristic of calcite (Chan et al., 2017). The few Ca sulfate spectra from Calama 031 are consistently combined with Ca carbonates (**Fig. 7b**).

3.3 Distribution and abundances of secondary minerals

The X-ray compositional map of LoV 123 reveals a high abundance of evaporites concentrated near the edge of the section, in the region adjacent to the fusion crust, but also shows Ca sulfate accumulation within porous inner regions of the chondrite (**Fig. 2**). In contrast, EM 464, Calama 031, and Paposo 088 display relatively homogeneous evaporite distributions across the analyzed areas. The average size of evaporite-bearing pores increases systematically from CAIs (7.8 ± 3.7 μm) to the matrix (7.9 ± 4.0 μm) and chondrules (11.5 ± 6.3 μm) and to Fe sulfide alteration zones (17.0 ± 9.7 μm; **Fig. 4b**).

Point-counting analysis of primary and secondary phases using SEM-EDS elemental maps is summarized in **Table 3**. The total modal abundance of evaporites (sulfates and

carbonates) is 2.5 ± 0.3 vol%, 2.8 ± 0.3 vol%, 1.4 ± 0.3 vol%, and 0.4 ± 0.2 vol% in LoV 123, EM 464, Calama 031, and Paposo 088, respectively. Ca sulfate is the dominant evaporite phase in LoV 123 and EM 464, reaching 2.5 ± 0.3 vol% and 2.5 ± 0.4 vol%, respectively. In contrast, Ca sulfate is nearly absent in Calama 031 (0.05 ± 0.05 vol%) and occurs in only minor amounts in Paposo 088 (0.5 ± 0.2 vol%). Ca carbonates were detected only in Calama 031 (1.4 ± 0.3 vol%) and EM 464 (0.3 ± 0.1 vol%). The mapped abundance of Fe oxide/oxyhydroxide phases, estimated from SEM-EDS compositional maps and BSE images, is 3.8 ± 0.4, 4.9 ± 0.5, 4.9 ± 0.5, and 8.2 ± 0.6 vol% in LoV 123, EM 464, Paposo 088, and Calama 031, respectively (**Table 3**). Fe-O-rich phases are not restricted to areas surrounding Fe-Ni metal, but also occur adjacent to Ca sulfates (**Fig. 3h**). No correlation was observed between the mapped abundance of Fe oxide/oxyhydroxide phases and evaporites.

4- Discussions

4.1 Origin of evaporites in the Atacama CO chondrites

Textural observations indicate that evaporites are widespread in CO chondrites from the Atacama Desert. In carbonaceous chondrites, evaporites may originate from either (i) pre-terrestrial fluid circulation during aqueous alteration on the parent body (Fredriksson and Kerridge, 1988; Airieau et al., 2005; Lee, 1993; Alexander et al., 2015; Chan et al., 2017; de Leuw et al., 2010) or (ii) secondary minerals produced by brine precipitation during terrestrial weathering (Velbel, 1988; Losiak and Velbel, 2011; Lee and Bland, 2004; Abreu and Brearley, 2005; Zurfluh et al., 2013). However, unlike CM, CR, or CI chondrites, COs experienced minimal aqueous alteration on their parent bodies (Marrocchi et al., 2018; Alexander et al., 2018). Consistently, most of the evaporites identified in this study are not

associated with phyllosilicate phases (e.g., Brearley, 1993), but with clear terrestrial weathering products such as Fe oxyhydroxides and weathered Fe sulfides (**Figs. 3-4**).

The Ca-S covariation observed in the semi-quantitative EDS data of LoV 123 is consistent with a paragenetic sequence involving Ca sulfate, Fe-bearing Ca sulfate, and jarosite-like phases (**Fig. 8**). In LoV 123, Ca sulfate in veins shows no systematic Ca-S trend, consistent with open-space precipitation from variably evolved fluids (Van Driessche et al., 2019). In contrast, Ca sulfates replacing Fe sulfide exhibit a strong negative Ca-S correlation, diagnostic of closed-front replacement at a reaction interface (**Fig. 8a**). Within the sulfide-weathering nodules, Ca sulfate, Fe-bearing Ca sulfate, and jarosite-like phases fall on a single mixing line (**Fig. 8b**). This is consistent with sub-micron intergrowths and progressive neutralization of initially acidic, sulfate-rich solutions (e.g., Bladh, 1982). These relationships connect jarosite-like phases formation to sulfide oxidation and the subsequent development of Ca sulfate precipitation during neutralization, consistent with the petrographic observations (**Figs. 3-5**).

Recent analyses of returned samples from Bennu revealed a complex evaporitic paragenesis linked to brine circulation, including Ca-, Mg-, and Na-carbonates, Mg- and Na-phosphates, Na-sulfides, Na-chlorides, and Na-fluorite (McCoy et al., 2025). Notably, this assemblage of evaporites does not include Ca sulfates, the most abundant evaporitic phases reported in our CO specimens as well as in other hot- and cold-desert finds (Velbel, 1988; Losiak and Velbel, 2011; Zurfluh et al., 2013; Lee and Bland, 2004; Lee et al., 2021). Furthermore, even in rapidly recovered fall chondrites such as Winchcombe (CM2), Ca sulfates and carbonates have been observed filling in secondary veins and pore spaces in the fusion crust only days after recovery (Jenkins et al., 2024). These observations suggest that Ca sulfates are among the earliest alteration products to precipitate in terrestrial settings, being facilitated by primary porosity, atmospheric humidity, and internal/external ion inputs

(Bland et al., 2006; Zurfluh et al., 2013; Lee et al., 2021). The prolonged terrestrial residence time of Atacama meteorites (up to ~2 Myr; Drouard et al., 2019; Soto et al., 2025), combined with their exposure to episodic moisture and oxidizing conditions, strongly supports a secondary terrestrial origin for the Ca sulfates identified in the CO chondrites analyzed. The texture and size distribution of evaporite-bearing pores in our samples (Fig. 4b) vary among different chondritic components, suggesting that Ca sulfates predominantly precipitated within pre-existing open pore spaces. The observed size variation likely reflects differences in porosity among components, together with later secondary modification either on the parent asteroid or terrestrial weathering (Lewis et al., 2018, 2019). Some sulfates in CM chondrites have been interpreted as pre-terrestrial in origin based on (i) their variable crystal habits within veins formed during multiple alteration events under different conditions (Lee, 1993), and (ii) oxygen-isotopic compositions that deviate from the terrestrial fractionation line in water-soluble sulfates extracted from CM2 chondrites ($\Delta^{17}O$ ranging from -0.23 ± 0.1‰ and 1.18 ± 0.1‰; Airieau et al., 2005). However, variable crystal habits can also arise under terrestrial conditions through successive episodes of dissolution and reprecipitation. Moreover, certain terrestrial sulfates of atmospheric origin can exhibit mass-independent oxygen isotope fractionation, which thus deviate from the terrestrial fractionation line. This occurs when sulfate forms through aqueous-phase oxidation of SO_2 in cloud or rain droplets, during which a mass-independent isotopic signature is transferred from atmospheric oxidants such as ozone and hydrogen peroxide (Savarino et al., 2000; Bao et al., 2000). Similar mass-independent fractionation of oxygen isotopes, with $\Delta^{17}O$ ranging from 0.17 ± 0.03 ‰ to 1.06 ± 0.06 ‰, has been reported in sulfate-rich soils from the Atacama Desert (Klipsch et al., 2023). This suggests that $\Delta^{17}O$ anomalies in sulfates detected on CM2 chondrites may potentially reflect a mixture with atmospheric inputs. However, water-soluble sulfates have not yet been extracted for the analysis of oxygen isotopes from CO chondrites, and it is

414 unclear whether these oxygen isotope signals are retained from the parent body or
415 overprinted during terrestrial residence.

416 Carbonates in Calama 031 occur as thick veins cutting across all chondritic
417 components with sharp, irregular interfaces (**Fig. 3e**). Although Ca carbonate minerals (e.g.,
418 calcite, aragonite, dolomite) can be common in aqueously altered CI, CM, and CR chondrites
419 (Alexander et al., 2015; Chan et al., 2017), they have not been reported previously in COs
420 (e.g., Doyle et al., 2015). Beyond primary porosity, evaporites commonly occupy secondary
421 veins, likely formed by thermal weathering and subsequent cracking of the meteorite in the
422 Atacama Desert (e.g., McKay et al., 2009). In Calama 031, which has a reported shock stage
423 of S2 (Gattacceca et al., 2020), some fractures may predate terrestrial weathering. This
424 inference is based on the meteorite shock classification and fracture context, rather than on
425 direct evidence of shock effects in the Ca-bearing phases (e.g., Kurosawa et al., 2022). These
426 pre-existing fractures could have been efficiently infilled by secondary minerals during fluid
427 circulation, facilitated by cation mobility into the meteorite interior through advection. While
428 our thick section did not expose any fusion crust, the main sample shows evidence of thick
429 veins of evaporites crossing the fusion crust (see photograph by Timur Kryachko in the
430 Encyclopedia of Meteorites (2018)). Furthermore, the vein morphology in our CO section
431 closely resembles secondary carbonate veins documented in the CV3 chondrites Leoville and
432 Vigarano (Abreu and Brearley, 2005). The terrestrial origins of the Ca carbonate veins in
433 Calama 031 are further supported by the sharp vein boundaries and the presence of embedded
434 chondrule and matrix fragments within the carbonate veins (**Fig. 3f**).

435 Several procedures applied during sample storage, preparation, or analytical
436 measurement may also induce alteration in meteorites (e.g., Bland et al., 2006; King et al.,
437 2020). Although Ca sulfates can be formed during curation through sulfide oxidation or
438 sulfate remobilization (Gounelle and Zolensky, 2001; Bland et al., 2006), multiple lines of

evidence indicate that the evaporites reported in the studied CO chondrites were already present before sample preparation: (i) the Ca sulfates in LoV 123 show identical textures and distributions by SEM-BSE imaging to those documented in previous SEM-EDS analyses (**Fig. S6**; Pinto et al., 2021); (ii) polishing scratches were visible on Ca sulfates in LoV 123 immediately after sample preparation; (iii) most sulfates identified in LoV 123, Calama 031, and EM 464 are anhydrite, which cannot form under the section's conservation conditions (1 atm and ~20°C; Van Driessche et al., 2019); and (iv) the different occurrence of evaporitic phases (i.e., Ca sulfates and Ca carbonates) in samples curated and transported together further indicates an origin before collection. Ca sulfate precipitation during storage may occur on relatively short timescales (a few years) under atmospheric conditions (King et al., 2020). However, multiple textural observations indicate that most of the sulfates described here were already present before sample preparation and curation. Overall, the textural, mineralogical, and comparative evidence supports an origin as pre-existing terrestrial alteration products of the meteorites.

A parent-body origin cannot be fully dismissed, but it is considered less likely for the Ca sulfates and associated Fe oxyhydroxides described here. CO chondrites evidence low aqueous alteration, and carbonates are generally absent from CO and CV chondrites (Doyle et al., 2015). Moreover, parent-body metasomatism in type 3 chondrites is typically expressed by alteration of matrix, chondrule mesostasis, and refractory inclusions, including replacement by phyllosilicates and formation of secondary fayalite, magnetite, and nepheline (Huss et al., 2006; Krot et al., 2025). Similarly, experimental studies of aqueous alteration on the CO3 chondrite Kainsaz indicate a production of matrix cementation and porosity decrease rather than late open-pore salt infilling (Suttle et al., 2022). In contrast, the phases described in the current samples occur as pore- and vein-filling evaporites associated with partial Fe sulfides alteration and Fe oxyhydroxides. Such an assemblage is more consistent with

terrestrial weathering in a hot desert environment, where sulfates, Ca carbonate, silica, and Fe oxyhydroxides are common secondary products (Lee and Bland, 2004; Gounelle and Zolensky, 2001; Jenkins et al., 2024).

Paposo 088 exhibits a notably low abundance of Ca sulfates (0.47 ± 0.15 vol%) compared with other CO chondrites recovered closer to the Pacific coast. This difference may result from the limited analyzed surface area, low porosity, section position within the main mass, or partial dissolution and reprecipitation during water-assisted polishing. Dissolution of gypsum occurs when water is undersaturated with respect to $CaSO_4 \cdot 2H_2O$. Experimental studies show that undersaturated conditions can induce surface retreat, roughening, and localized dissolution features on gypsum, although the exact morphology depends strongly on surface state and experimental conditions (Fan and Teng, 2007; Lennaerts, 2013). In polished sections such as those studied here, these experimental observations are not directly resolvable at the scale of the SEM images (**Fig. 3g,h**). We therefore interpret the textures in Paposo 088 as evidence for partial dissolution or incomplete preservation of Ca sulfate pore fillings. In addition, the hand sample displays a rusty exterior and lacks a fusion crust, unlike the other CO specimens analyzed. If Paposo 088 represents the most weathered meteorite in this set, its restricted Ca sulfate distribution may reflect either (i) precipitation of secondary evaporitic phases during polishing in localized pore networks, or (ii) pre-existing heterogeneity of Ca sulfate confined to semi-connected pore systems, as observed in the interior of LoV 123 (**Fig. 2**). Recent cosmogenic ^{36}Cl measurements on a suite of CO chondrites from the Atacama Desert indicate that Paposo 088 is among the oldest Atacama meteorites, with a terrestrial age of 2183 ± 95 kyr (Soto et al., 2025). This long residence time likely promoted successive dissolution-reprecipitation of Ca sulfate within semi-connected pore networks, further decoupling present-day evaporite distribution from their early post-fall abundances.

Considering all the presented evidence, including our petrographic description, comparison with pre- and post-terrestrial evaporites reported in other carbonaceous chondrites, and the prolonged terrestrial exposure of Atacama meteorites, the formation of Ca sulfates and Ca carbonates through terrestrial weathering processes in the Atacama Desert is supported for all CO3 chondrites studied here.

4.2 Differences between evaporitic assemblages across meteorite recovery areas

Having established that the evaporitic minerals in the Atacama CO chondrites are of terrestrial origin, a main question concerning the sources of calcium, carbonate, and sulfate ions involved in their formation arises. Two reservoirs can be considered: (i) intrinsic mineral phases within the carbonaceous chondrites, and (ii) external inputs derived from terrestrial soils. Notably, our point count analysis reveals different variations in the evaporite assemblages across different Atacama COs. Calama 031, recovered near the Western Cordillera, contains 1.4 ± 0.3 vol% of Ca carbonates, whereas samples collected closer to the Pacific coast show significantly lower values (<0.3 ± 0.1 vol%). On the other hand, EM 464 and LoV 123 exhibit higher Ca sulfate abundances (2.5 ± 0.4 and 2.5 ± 0.4 vol%, respectively), while Calama 031 contains only 0.05 ± 0.05 vol% (**Table 3**).

Under the oxidizing conditions of the Atacama Desert, CO chondrite minerals are far from chemical equilibrium, promoting weathering and mobilization of cations and anions within the meteorite interiors. Calcium, the dominant cation in both carbonates and sulfates, can originate from several meteoritic phases, including the mesostasis of Mg-rich chondrules (up to ~20 wt.% CaO; Tomeoka and Itoh, 2004) and Ca rich phases in CAIs (e.g., melilite, hibonite, perovskite; MacPherson, 2014). Minor CaO is also present in Fe-rich olivines (~0.3 ± 0.2 wt%; Pinto et al., 2024a), which may locally contribute to the formation of Ca sulfates

515 inside Fe-rich chondrules **(Fig. 5e-f)**. Although CO chondrites contain <1.5 wt.% total carbon
516 (Grady and Wright, 2003; Pearson et al., 2006), most of the calcium and carbon required for
517 the Ca carbonate formation resides in chondrules and the matrix (e.g., Ebel et al., 2016;
518 Pearson et al., 2006). Given that all analyzed samples belong to the same class (CO
519 chondrites) and display comparable proportions of chondrules, CAIs, and matrix (**Table 3**),
520 the observed variation in evaporite types cannot be explained solely by differences in primary
521 mineralogy.

522 Troilite oxidation provides an additional source of sulfate ions (Bland et al., 2006;
523 Velbel et al., 2012; Zurfluh et al., 2013). In all CO chondrites, troilite oxidation has been
524 associated with Ca sulfate precipitation, suggesting that sulfide hydrolysis is a local supplier
525 of SO_4^{2-} ions. The hydrolysis reaction releases hydrogen ions, decreasing pH and enhancing
526 the dissolution of nearby silicates and metals (Velbel et al., 2012). The consequent release of
527 cations into solution facilitates further sulfate precipitation. Variations in terrestrial residence
528 time may also have contributed to these differences, because repeated wetting-drying,
529 dissolution, and reprecipitation can progressively modify the secondary weathering
530 assemblage. Recent preliminary ^{36}Cl ages for Atacama CO3 chondrites range from ~102 ± 74
531 kyr for LoV 123 to ~2183 ± 95 kyr for Paposo 088 (Soto et al., 2025), indicating potentially
532 large differences in the duration of terrestrial alteration. In this context, the high Ca sulfate
533 abundance in LoV 123 and the very low evaporite abundance in Paposo 088 may reflect
534 progressive remobilization of secondary phases during prolonged residence on the Atacama
535 surface.

536 Calama 031 was recovered from the Opache Formation, composed of marsh
537 limestones, sandy limestones, and calcareous conglomerates (Tomlinson et al., 2018). The
538 depleted $\delta^{18}O$ signature of the local limestones suggests precipitation from ponding
539 groundwater during the Miocene-Pliocene (de Wet et al., 2015). The carbonate-bearing veins

in Calama 031 were likely formed by the infiltration of CO_2-rich aqueous solutions that had leached Ca^{2+} ions from surrounding limestone, later percolating through the meteorite fractures. Our petrographic observations indicate that (i) fractures are only partially filled, (ii) veins exhibit incomplete carbonate infill, and (iii) displaced chondrule fragments remain close to their original positions (**Fig. 3f**). These features imply multiple episodes of dissolution-reprecipitation in near-static pore waters (e.g., Lee, 1993; Abreu and Brearley, 2005).

The case of the Tatahouine meteorite supports this interpretation: 63 years after its fall in Tunisia, secondary carbonates were found filling veins and pores that had been present as voids in the freshly recovered material (Barrat et al., 1998). The $\delta^{13}C$ signature of these carbonates reflected derivation from the local limestone-rich soil. This shows that terrestrial carbonates can precipitate rapidly when calcareous substrates are abundant at the fall site and moisture is accessible. The Calama area has a relatively high mean annual precipitation (~30 mm/yr; Pinto et al., 2024b) compared with other parts of the Atacama, increasing to ~50 mm/yr along its eastern margin (Rech et al., 2006). These seasonal rains are linked to the South American summer monsoon, which has transported varying amounts of Atlantic moisture over the Andes since at least the late Pleistocene-Holocene (Rech et al., 2006; González-Pinilla et al., 2021). Episodic high-precipitation events likely generated supersaturated calcareous fluids during interaction with limestone bedrock, affecting meteorites in the region in both past and present conditions. These fluids infiltrated the meteorite through fractures and interconnected pores, driving repeated cycles of evaporation and carbonate precipitation.

El Medano 464 and Paposo 088 were recovered within the La Negra Formation of the Coastal Range, approximately 17 km apart along a north-south transect. This unit consists of andesitic to basaltic lavas interbedded with red sandstones and volcanic breccias (Álvarez et

565 al., 2016). LoV 123 was recovered approximately 24 km inland from EM 464, on Miocene-
566 Pleistocene alluvial deposits of the Central Depression (Espinoza et al., 2012). Gypsum
567 ($CaSO_4 \cdot 2H_2O$) is one of the most abundant evaporitic minerals in coastal soils, extending
568 inland toward the Central Depression and reaching high concentrations at 24-25°S latitude
569 (Voigt et al., 2020; Rech et al., 2003). Compared with other salts, Ca sulfates are moderately
570 soluble and generally better preserved in the Atacama surfaces. Geochemical data for the
571 local soil indicate sulfate concentrations of 20-40 wt.% near Paposo DCA, decreasing to < 20
572 wt.% in the Central Depression (Voigt et al., 2020). This spatial trend implies that Atacama
573 soils provided high external SO_4^{2-} availability for Ca sulfate formation in EM 464, Paposo
574 088, and LoV 123. The El Médano, Paposo, and Los Vientos DCAs experience mild annual
575 temperatures (~15-17 °C) with extremely low annual averages precipitation (≤ 10-15 mm/yr;
576 Larrain et al., 2002; Pinto et al., 2024b). By contrast, fog collectors at Paposos (750 m a.s.l.)
577 record mean fog-water inputs of 3.36 mm/day (~1225 mm/yr), thus hydrologic inputs are
578 dominated by fog rather than rain on these DCAs (Larraín et al., 2002; Sun et al., 2024).
579 Furthermore, marine aerosols represent a major sulfate source along the coast (Ericksen,
580 1981; Rech et al., 2003). Sulfur isotope data confirm that this marine influence decreases
581 inland (Rech et al., 2003), resulting in progressively sulfate-depleted brines within eastern
582 DCAs of the Central Depression. Additionally, weathering of andesitic and basaltic rocks
583 may locally contribute sulfate to Atacama soils on smaller spatial scales (Voigt et al., 2020).
584 Taken together, these observations suggest that the contrasting evaporitic assemblages
585 in the Atacama COs primarily reflect site-specific environmental conditions rather than
586 differences in meteoritic composition. In Calama 031, calcium and carbonate ions derived
587 from calcareous soils precipitated as carbonates under higher rainfall conditions, where
588 sulfate was either less available or actually buffered by an excess of carbonate. In contrast,
589 near-coastal meteorites such as EM 464, Paposo 088, and LoV 123 accumulated sulfates

through repeated exposure to sulfate-rich brines and oxidative weathering in drier, Ca sulfate-dominated terrains. These findings highlight the importance of local soil geochemistry and microclimatic gradients in controlling terrestrial alteration pathways of meteorites across (hyper)arid environments.

4.3 Terrestrial anhydrite vs gypsum in Atacama meteorites

Micro-Raman spectroscopy of the secondary evaporitic assemblages in the CO chondrites indicates that the dominant Ca sulfate polymorph is anhydrite ($CaSO_4$). Multiple spot and line analyses of secondary Ca sulfates in Calama 031, LoV 123, and EM 464 consistently yield spectra lacking O-H stretching bands in the 3400-3500 cm^{-1} region, confirming the absence of structural water. Comparison with reference spectra of natural gypsum (Pellenberg, Belgium) and anhydrite (Kłodawa, Poland) shows a closer match to anhydrite, with no spectral evidence of laser-induced dehydration (**Fig. S2**), thereby ruling out analytical artifacts such as beam heating (e.g., Lee, 1993; King et al., 2020). In some Ca sulfates associated with Fe sulfides or Fe oxyhydroxides, the $\nu_1(SO_4)$ stretching mode occurs near 1015 cm^{-1}, a position that could indicate the presence of bassanite (Prieto-Taboada et al., 2014). However, as mentioned before this minor shift may result from cationic impurities (e.g., Fe^{2+}, Mg^{2+}, or Na^{+}) that substitute within the sulfate lattice, which can displace Raman peak positions by 1-2 cm^{-1} toward lower wavenumbers (e.g., Chan et al., 2017). These results demonstrate that the secondary Ca sulfates identified in meteorites are genuinely anhydrous, with no evidence of gypsum or bassanite intermediates (Prieto-Taboada et al., 2014). The chemical heterogeneity of anhydrite in secondary veins (**Fig. 8a**) suggests complex alteration influenced by Atacama soils and coastal fog, which is consistent with formation under low water activity.

615 The predominance of anhydrite in these meteorites is remarkable because, under most
616 terrestrial evaporitic conditions, gypsum is the stable phase, whereas anhydrite formation is
617 kinetically and thermodynamically restricted (Ossorio et al., 2014; Van Driessche et al.,
618 2019). Only under extremely arid and warm conditions, such as those found in saline flat or
619 salt-crusted depression (i.e., sabkha environments), has anhydrite been observed to form
620 directly from brines or as a replacement of gypsum (Butler et al., 1982; Aref and Taj, 2018).
621 Calcium sulfate precipitation experiments using water-organic (co)solvent mixtures with
622 concentrated H_2SO_4 demonstrate that phase-pure anhydrite forms only at < 0.2 wt% H_2O,
623 while slightly higher water contents (0.43-4.14 wt%) produce anhydrite-bassanite mixtures or
624 phase-pure bassanite (Tritschler et al., 2015). Importantly, kinetic constraints derived from
625 hydrothermal and solution experiments show that gypsum can remain persistent in metastable
626 form even at elevated temperatures in the absence of appropriate nuclei. In pure water
627 without anhydrite seeds, gypsum remains stable up to ~90 °C for at least 20 days (despite a
628 theoretical stability limit near 45-50 °C), whereas transformation accelerates at higher
629 temperatures (100% hemihydrate at 150 °C; 100% anhydrite at 200 °C after 4 h) and is
630 catalyzed by anhydrite seeding (Azimi and Papangelakis, 2011). The same study
631 demonstrated that solution chemistry strongly modulates pathways. For instance, sulfuric
632 acid promotes transformation below and above 100 °C (e.g., 1.5 M H_2SO_4 at 90 °C achieves
633 full conversion to anhydrite in 1 day), and NaCl accelerates transformation through chloride
634 content that enhances gypsum dissolution (< 100°C) without the immediate production of
635 hemihydrate. These kinetic-chemical controls correspond with Atacama microenvironments,
636 where chloride-nitrate-rich solutions of low water activity favor slow, solution-mediated
637 reprecipitation of anhydrite over gypsum at ≤ 42 °C (Van Driessche et al., 2019; Voigt et al.,
638 2020; Charola et al., 2007). This can explain impurity-bearing anhydrite in veins and cavities
639 of CO chondrites without invoking high surface temperatures. Over long timescales, Atacama

conditions favor dissolution-reprecipitation mechanisms, rather than dry thermal dehydration, as the dominant pathway for anhydrite stabilization (Voigt et al., 2020; Arens et al., 2021).

Nevertheless, the possibility of biogenic mediation in the gypsum-anhydrite transformation cannot be dismissed (e.g., Al Disi et al., 2023; Huang et al., 2020). Recent studies have shown that endolithic cyanobacteria inhabiting gypsum in the Atacama Desert extract water from the mineral lattice to sustain metabolic activity, thereby converting gypsum into anhydrite through biofilm-mediated dissolution and precipitation of nanocrystalline anhydrite (Huang et al., 2020). Experiments conducted under controlled dry conditions confirm that the extent of transformation correlates with microbial abundance, whereas no change occurs under hydrated conditions. This biologically driven pathway offers a plausible mechanism for anhydrite formation within meteorites exposed to desertic conditions, where microbial colonization may exploit mineral-bound water. Although no microorganisms were found in this study, the detection of organic-related Raman bands in EM 464 and LoV 123 further reinforces this link. Several spectra of Ca sulfate-bearing regions display the first-order D (~1350 cm^{-1}) and G (~1580 cm^{-1}) bands characteristic of disordered carbonaceous material (Tuinstra and Koenig, 1970a,b), which can be used by microorganisms in catabolic processes. Control analyses of the embedding resin show no evidence of thermally induced carbon bands, and samples were consistently repolished after SEM analysis to remove the carbon coating, making contamination from residual coating or epoxy degradation unlikely. Previous molecular and isotopic analyses of EM 464 reveal abundant organic compounds dominated by acyclic hydrocarbons, carboxylic acids, and alcohols with $\delta^{13}C$ values between -27.8‰ and -27.5‰, typical of terrestrial biosignatures associated to post-fall microbial colonization (Pinto et al., 2025). Such colonization likely exploited the evaporitic niches, such as Ca sulfate and carbonate cavities, which provide microenvironments capable of retaining trace water and nutrients.

665

666 **4.4 Implications for Martian Environments**

667

668 The mineralogical and chemical characteristics of the Atacama CO chondrites provide
669 valuable analogs for understanding carbonate and sulfate formation and preservation on Mars
670 (**Fig. 9**). Both environments are strongly oxidizing, extremely dry, and characterized by
671 processes that concentrate salts, but only the Atacama operates under Earth-like pressure and
672 hosts an active near-surface biosphere (Azua-Bustos et al., 2022). Within this atmospheric
673 and climatic context, the Atacama CO chondrites record how short-lived brine pulses interact
674 with meteoritic material in a Mars-analogue hyperarid environment. Oxidation of Fe sulfide
675 produces jarosite, Fe oxyhydroxides (including hematite), and Ca sulfate, analogous to
676 reported jarosite/hematite/Ca sulfate facies associations on Mars (Madden et al., 2004; Tosca
677 et al., 2008; Tosca and McLennan, 2009). In this context, the composition and pH of the
678 fluids and substrates play a key role in controlling the resulting secondary mineral
679 assemblages. Micro-Raman data identify anhydrite as the dominant Ca sulfate (ν_1~1017 cm^{-1},
680 no OH bands) in CO chondrites, similarly to how it has been reported on the Gale Crater
681 using X-ray diffraction data (Vaniman et al., 2018; Vaniman et al., 2024). In two CO
682 chondrites studied here, D-G bands occur along some of the Ca sulfate veins, indicating
683 carbonaceous matter trapped in secondary minerals and providing a process analogue for the
684 spatial coupling between organics and redox-sensitive conditions documented in Jezero
685 Crater mudstones (Hurowitz et al., 2025).

686 In this study, CO chondrite data provide two observations relevant to evaporite
687 formation in hyperarid saline systems. First, the dominance of anhydrite over gypsum and
688 bassanite is consistent with low-water-activity brines, because increasing salinity extends the
689 stability field of anhydrite to lower temperatures (Harvie et al., 1980; Van Driessche et al.,

690 2019; Voigt et al., 2020; Wehmann et al., 2023). This interpretation is also consistent with
691 observations from Atacama soils, where anhydrite is associated with chloride- and nitrate-
692 rich settings and with secondary dissolution-reprecipitation processes (Voigt et al., 2020).
693 Second, our EDS maps show that the Ca sulfates contain minor Fe, Si, Cl, and P, suggesting
694 that impurity incorporation may have influenced their rehydration behavior and metastability,
695 as described for $CaSO_4$ phases in hyperarid terrestrial settings (Ossorio et al., 2014; Voigt et
696 al., 2020) and Martian meteorites (MIL 03346; Shi et al., 2022). These comparisons are
697 intended at the level of process rather than as a direct lithologic analogy with Martian rocks.
698 Overall, our results suggest that the resulting secondary assemblage is controlled primarily by
699 local conditions, particularly brine chemistry and substrate-derived ions. In the CO chondrites
700 studied here, Ca was likely supplied by local Ca-bearing primary phases within the meteorite,
701 although their contribution to evaporite formation appears to have been limited relative to
702 that of the surrounding terrestrial environment. In Martian systems, local Ca-bearing phases
703 such as plagioclase (e.g., Phillips et al., 2025) may likewise represent important Ca reservoirs
704 for the development of secondary alteration assemblages.

705 Recent observations of mineral-organic material coupling at Jezero further support
706 this model. Redox-linked associations among Fe-, S-, and P-bearing phases and organic
707 signals imply repeated fluid pulses and oxidation steps (Hurowitz et al., 2025). The Atacama
708 COs show how anhydrite formed under oxidizing, water-limited conditions, which can trap
709 and shield organics within microcavities and provide a physical substrate for preservation
710 during dry-wet cycling. Endolithic processes in the Atacama Desert can convert gypsum to
711 anhydrite by biofilm-mediated water extraction (Huang et al., 2020; Al Disi et al., 2023).
712 However, other non-biological redox gradients could also drive the same recrystallization and
713 stabilization. Oxidation of sulfide-bearing microdomains can locally generate sulfate and
714 acidity, promote dissolution of nearby Ca-bearing phases, and, after diffusion/mixing with

adjacent pore waters, induce renewed Ca sulfate supersaturation and reprecipitation. Organic signals strengthen the case of trapped carbon-rich material within sulfate precipitation. The D-G bands occur along veins, with parameters matching disordered insoluble organic matter in CO chondrites (Busemann et al., 2006; Bonal et al., 2016). Thus, Ca sulfate formation can trap meteoritic insoluble organic matter during water-limited alteration and potentially shield it from oxidation. Similar pairings at Jezero should be interpreted within a full mineral-redox context (e.g., Hurowitz et al., 2025).

From these lines of evidence, we propose similar large-scale processes on Mars: (i) jarosite-like phases, goethite and hematite should occur proximal to former Fe sulfides and grade outward to Ca sulfate; (ii) veins are expected to be compositionally heterogeneous, whereas secondary mineral replacement of Fe sulfides should produce systematic Ca-S trends; (iii) anhydrite will be relatively common where water activity was low, with gypsum restricted to locally wetter areas; and (iv) organics and other materials may become locally concentrated within secondary sulfates, particularly in microcavities, although in our dataset these occurrences are limited (17.1% of Ca sulfate spectra in EM 464 and 5.7% in LoV 123). Targeting evaporites and using the $\nu_1(SO_4)$ band as a humidity tracer may help reconstruct past water activity, pH, and redox conditions, as well as detect potential trapped organic matter, whether biological or not, across evaporite-rich areas on Mars.

5- Conclusions

We characterized evaporites in four CO carbonaceous chondrites from different dense collection areas of the Atacama Desert. Sulfates and carbonates occur as pore/vein infills, as well as replacements of Fe sulfide. Supported by the petrographic features and their systematic association with Fe oxyhydroxides, the evaporite assemblages suggest a terrestrial origin rather than a parent-body hydrothermal alteration. Variations in evaporite assemblages

in CO chondrites found across different dense collection areas reveal that they are largely controlled by local microclimates and soil chemistries rather than primary lithology composition. In Calama 031, Ca and carbonate ions likely derived from surrounding limestone that are subsequently precipitated as carbonate-bearing veins under sporadic rainfall events. In contrast, near-coastal CO chondrites such as EM 464, Paposo 088, and LoV 123 accumulated sulfates through repeated exposure to sulfate-rich brines from the Pacific Ocean and oxidative weathering in a Ca sulfate-dominated soil. Two recurrent Ca sulfate precipitations are observed: (i) sulfide-replacement showing an anticorrelation between Ca and S, and (ii) secondary infill veins with no correlation between Ca and S. Both precipitation modes commonly coexist within a single section. Raman signals reveal that Ca sulfate is dominated by anhydrite, consistent with precipitation from very low aqueous H_2O brines during prolonged wet-dry periods. This terrestrial anhydrite is likely generated by dissolution-reprecipitation rather than by high-temperature surface dehydration, which is consistent with anhydrite stabilization over long time scales in the Atacama soils. Furthermore, Raman signals of insoluble organic matter concentrate within Ca sulfate microcavities, implying trapping and potential preservation of organics, whether abiotic or biotic. Our petrography, Raman, and chemistry information of evaporite assemblages may serve as comparisons at the level of alteration process for evaporite-rich areas on Mars. This suggests that anhydrite would predominate at low water activity in Martian environments, and jarosite-like phases, goethite and hematite is expected near sulfide-rich zones. This approach could also reveal organic matter, even if non-biological, trapped within evaporite-rich areas on Mars.

Acknowledgments

We are grateful to Rodrigo Martínez (Museo del Meteorito), Juan Pablo Pizarro, and Timur Kryachko for access to the CO carbonaceous chondrites and their pictures. Thanks to Herman Goethals for his expert advice and technical assistance with the Raman analyses at RBINS. KS and AC thanks to the Electronic Microscopy Unit of UACh. in particular the technical support of Dagoberto Boisier. We also thank Dr. Paolo Sossi for editorial handling of the manuscript and Dr. Marina Martínez and an anonymous reviewer for their suggestions that improved the manuscript. This work was supported by the Belgian Science Policy (Belspo) Brain-Be DESIRED project to SD, SG and VD. VD is a Research Director of the Fonds de la Recherche Scientifique-FNRS. SG acknowledges the support of the VUB Strategic Research Program and VUB Large Research Group funding. GP acknowledges support as a Chargé de Recherche of the Fonds de la Recherche Scientifique-FNRS.

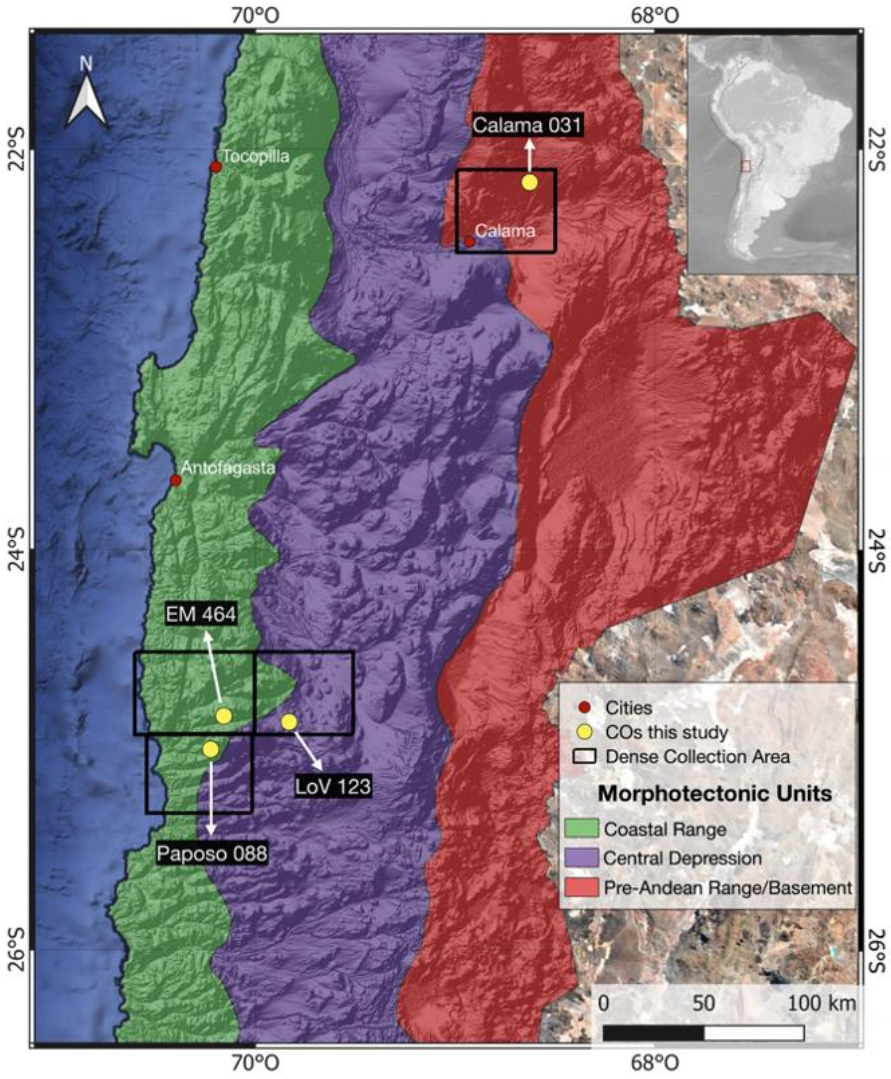

Fig. 1. Locations of the CO chondrites analyzed in this study are shown on a satellite basemap of northern Chile (Atacama Desert). Colors indicate the main morphotectonic provinces: Coastal Range (green), Central Depression (purple), and Pre-Andean Range/Basement (red). Yellow circles mark the find sites of EM 464, LoV 123, Paposo 088, and Calama 031, while red dots indicate nearby cities. Black rectangles delimit dense collection areas for meteorite recovery. Note that EM 464, LoV 123, and Paposo 088 occur near the Coastal Range-Central Depression boundary, whereas Calama 031 lies further east near Calama within the Pre-Andean province. Adapted from Pinto et al. (2024b).

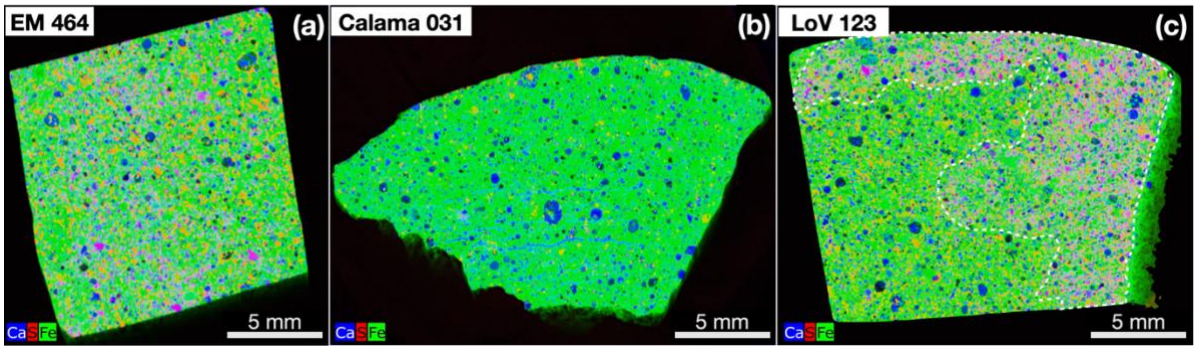

Fig. 2. Whole-section μ-XRF elemental maps of three studied CO chondrites. (a) EM 464, (b) Calama 031, and (c) LoV 123. The maps are shown in RGB color coding (Ca = blue, S = red, Fe = green). Green colors reflect the dominance of Fe-bearing silicates and opaque phases, whereas magenta indicates spatial association of Ca and S, consistent with Ca sulfates. White dotted outlines in LoV 123 delineate domains enriched in Ca sulfate phases. The maps highlight inter-sample differences in the abundance and distribution of evaporites.

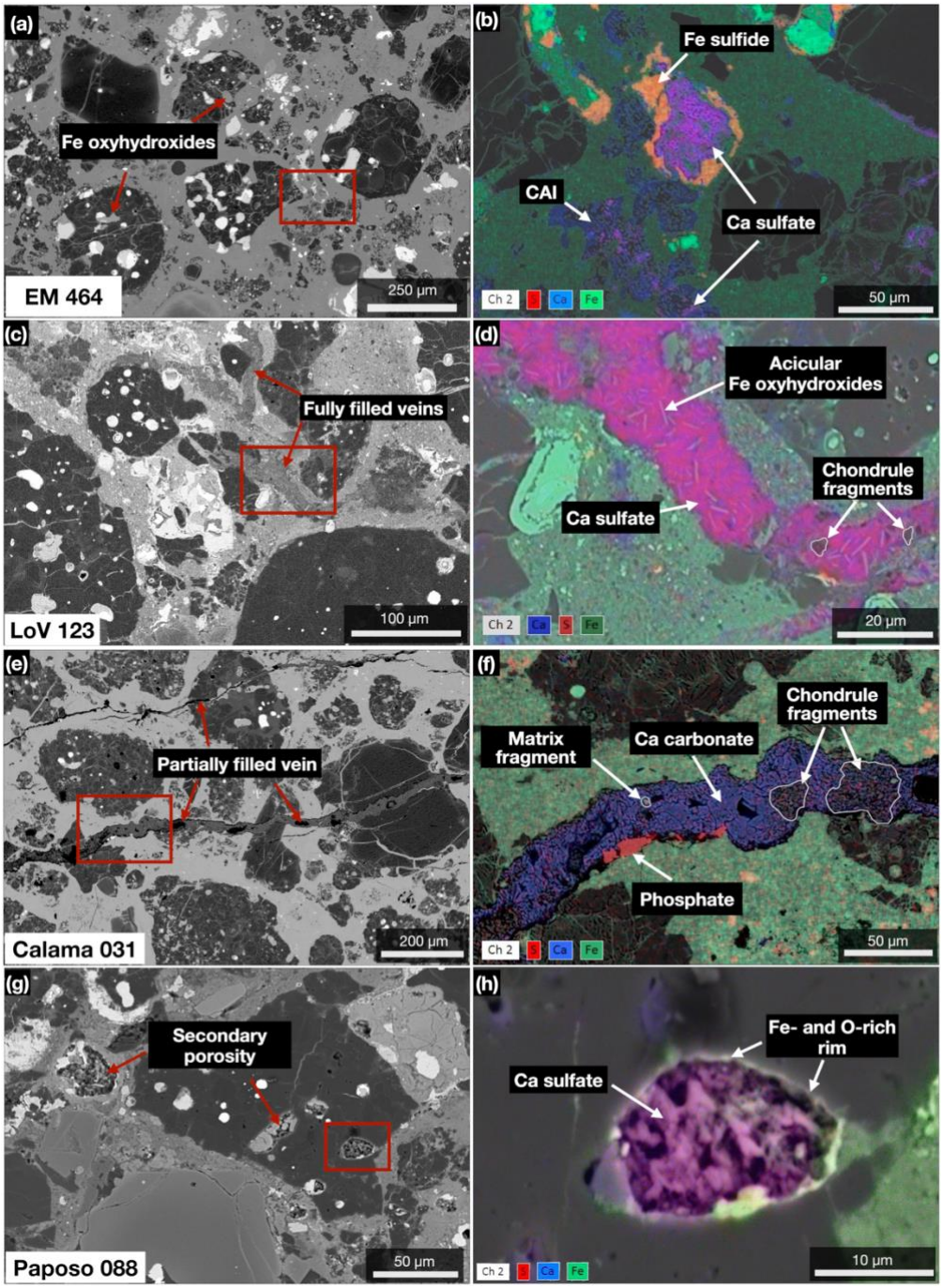

Fig. 3. Backscattered-electron (BSE) images and X-ray maps showing secondary alteration products in the studied CO chondrites. (a) EM 464 shows an overall chondritic texture with no abundant secondary veins but widespread Fe oxyhydroxides in chondrules and matrix. (b) Zoom of the red box in (a) showing a weathered Fe sulfide, chondrule, and Ca-Al-rich inclusion (CAI) with secondary Ca sulfate patches. (c) LoV 123 showing secondary veins completely filled with Ca sulfate, while the magnified area (d) reveals acicular Fe oxy/hydroxides (mainly goethite) intergrown with Ca sulfate. (e) Calama 031 showing a fractured texture with two veins partially filled by Ca carbonates. (f) Zoom of the Ca carbonate veins showing small P-rich grains as well as immersed chondrule and matrix fragments. (g) Paposo 088 showing secondary porosity in chondrule and metal grains (h) Zoom of (g) onto a deep Ca sulfate grain with high porosity and surrounded by an Fe- and O-rich phase rim. The X-ray maps display S in red, Fe in green, and Ca in blue (RGB). Mixed colors indicate Ca sulfate in magenta and sulfides in orange.

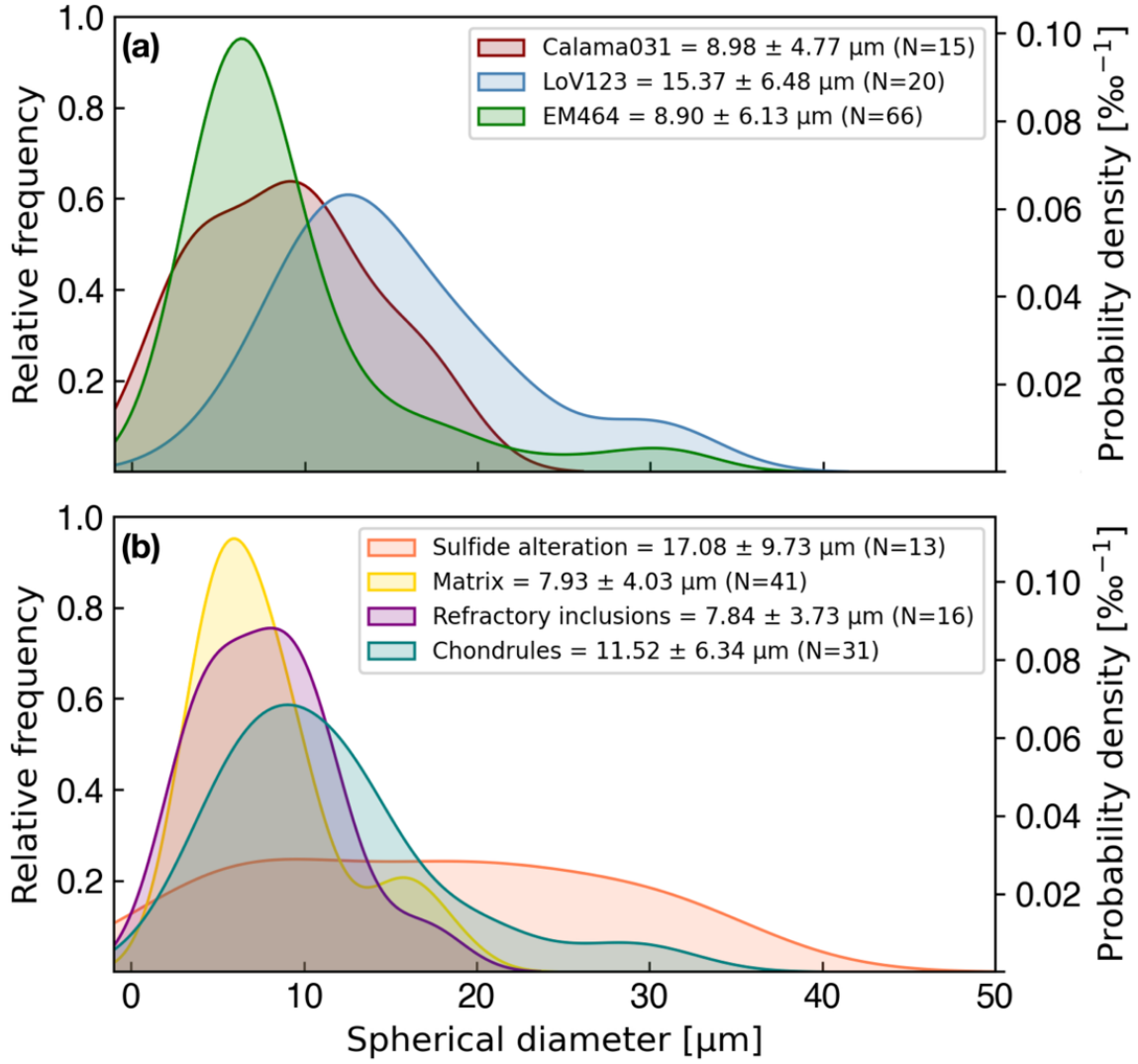

Fig. 4. Size distributions of evaporite-bearing pores measured in three CO chondrites. (a) Kernel-density estimates (KDEs) for each CO indicating that LoV 123 hosts significantly coarser-filled pores than Calama 031 and EM 464. (b) KDEs for each main chondritic component indicating that spherules related to sulfide alteration are the largest, which show no specific distribution. In contrast, those in the matrix and refractory inclusions (i.e., CAIs) are finer, consistent with the primary porosity of these compounds. The relative frequency is normalized to 1, and the right axis shows the corresponding probability density.

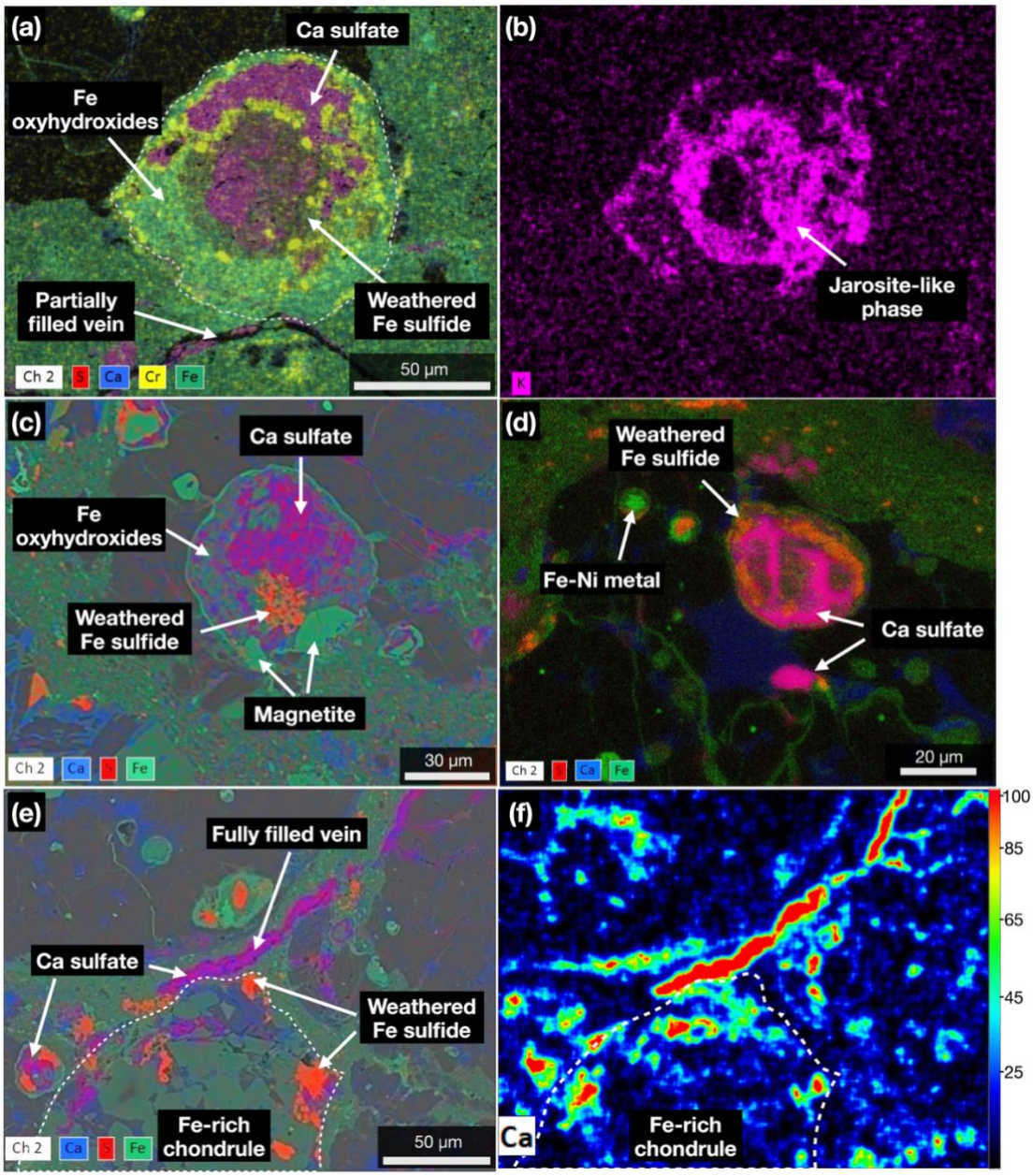

Fig. 5. X-ray compositional maps of weathered Fe sulfides and associated secondary phases in EM 464 (a-b) and LoV 123 (c-f). (a) A rounded clast hosts a core of weathered Fe sulfide replaced by jarosite-like phase, surrounded by Fe oxyhydroxides and containing irregular Ca sulfate associated with Cr-rich domains. A partly filled secondary vein occurs immediately below the altered grain. (b) K X-ray map of the same area shown in (a), highlighting the distribution of the jarosite-like phase within the altered sulfide assemblage. (c) A weathered Fe sulfide partly replaced by Ca sulfate and associated with Fe oxyhydroxides and magnetite grains along its margins. (d) Altered Fe sulfide grain, located in the interior of a Mg-rich chondrule, occurs in close association with Ca sulfate and adjacent non-altered Fe-Ni metal grains. (e) Ca sulfate occurs together with weathered Fe sulfides inside intercrystalline pores within an Fe-rich chondrule, as well as in a fully filled vein cross-cutting immediately above the chondrule. (f) Ca intensity map of the same area shown in (e), emphasizing the distribution of Ca-rich secondary phases around the chondrule margin and the slight Ca enrichment in the mesostasis of Fe-rich and Mg-rich chondrules. The X-ray maps display S in red, Fe in green, and Ca in blue, (RGB). Mixed colors indicate Ca sulfate in magenta and sulfides in orange.

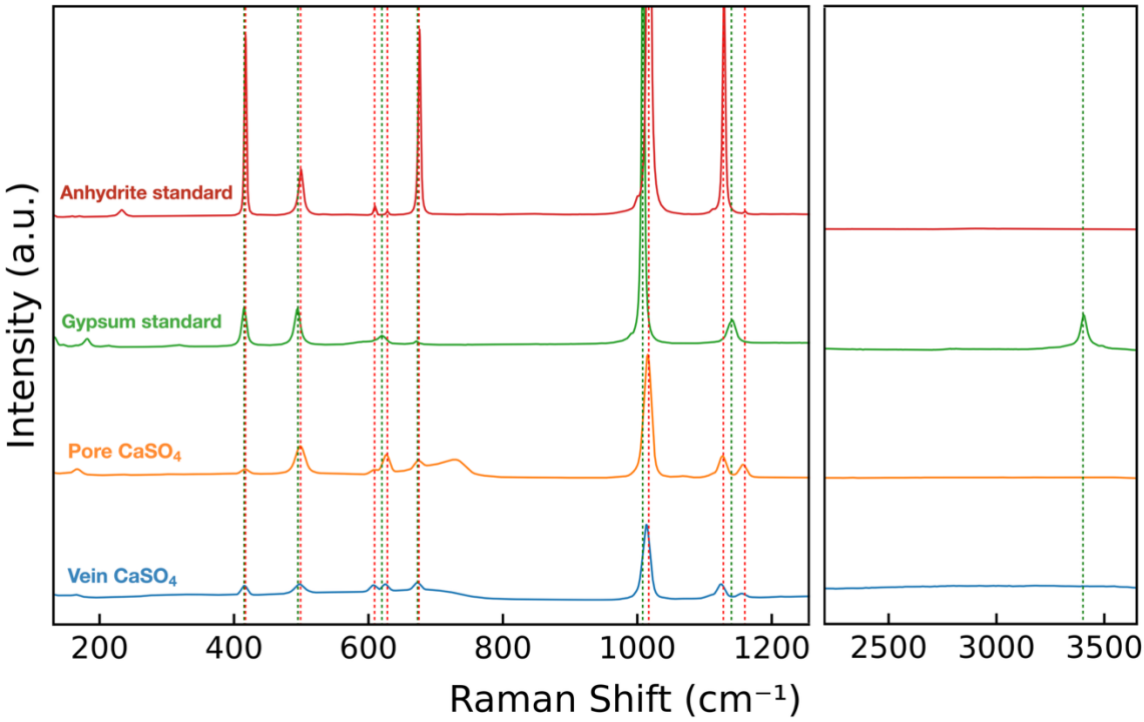

Fig. 6. Raman spectra showing the vibrational bands of SO_4 and H_2O of the reference standards and two selected $CaSO_4$ locations in LoV 123. The measured peak positions are compared with reference spectra of anhydrite (red dotted lines) at 417, 499, 609, 628, 675, 1017, 1111, 1128, and 1160 cm^{-1}, and gypsum (green dotted lines) at 415, 495, 620, 673, 1008, 1140, 3401, and 3491 cm^{-1} (Prieto-Taboada et al., 2014). The $CaSO_4$ spectra from LoV 123 closely align with the anhydrite standard peaks, confirming the presence of anhydrite.

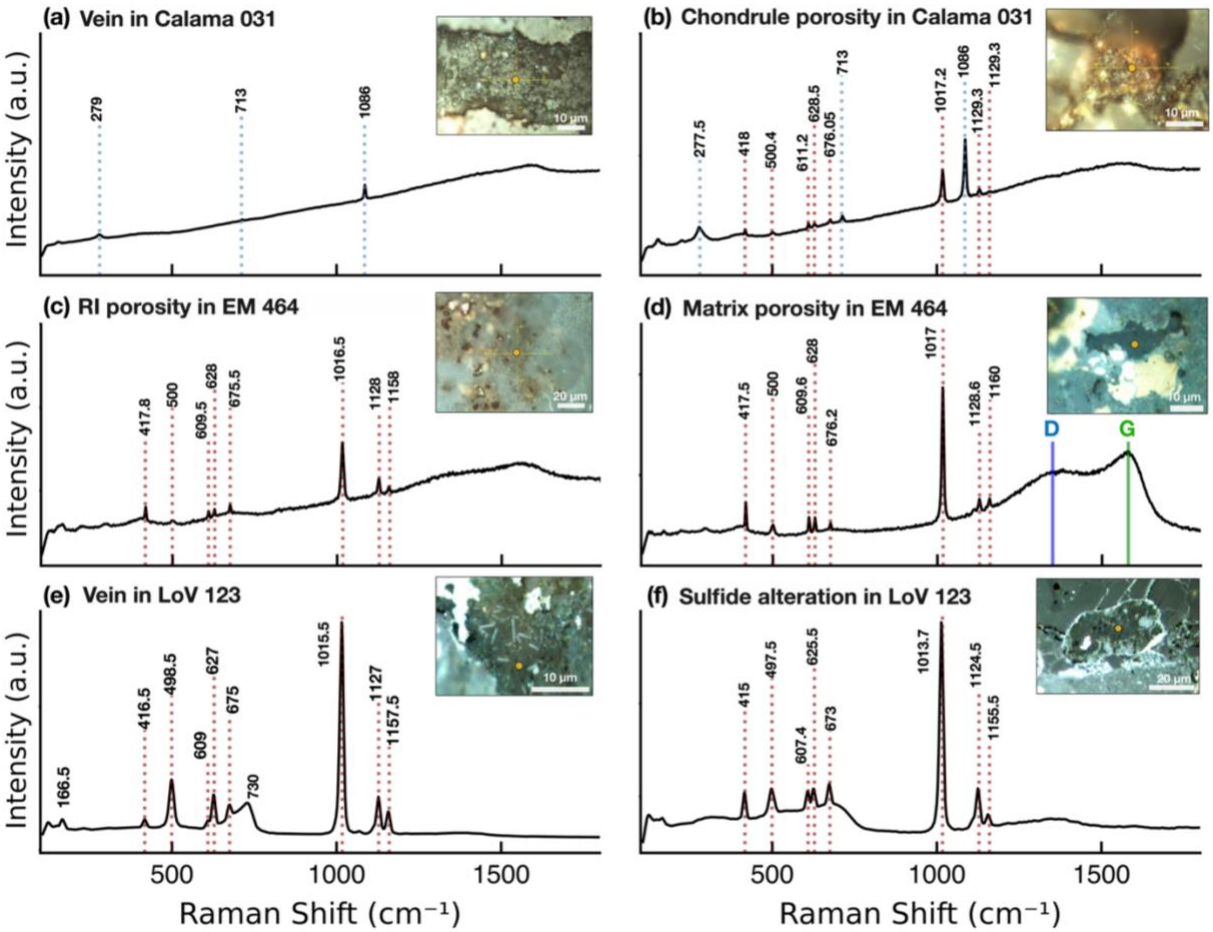

Fig. 7. Representative Raman spectra of evaporitic phases (Ca carbonates and Ca sulfates) with reflected-light micrographs of the analyzed spots (orange spot, not to scale). Panels (a-b) are from Calama 031, (c-d) from EM 464, and (e-f) from LoV 123. (a) Ca carbonate-filled vein. (b) Chondrule porosity hosting intergrown Ca sulfate and Ca carbonate. (c) Ca sulfate infilling a porous region within a refractory inclusion (RI). (d) Matrix porosity showing Ca sulfate together with disordered carbon, evidenced by the D (~1350 cm^{-1}) and G (~1580 cm^{-1}) bands. (e) Vein containing Ca sulfate with Fe oxyhydroxides. (f) Ca sulfate precipitated within weathered troilite. Sulfate bands are marked by red dashed lines with lattice of ν_2 at 415-500 cm^{-1}, ν_4 at 600-690 cm^{-1}, and ν_1-ν_3 at ~1015-1017 and ~1127-1160 cm^{-1}. Carbonate bands are indicated by blue dashed lines with lattice at ~279 and ~713 cm^{-1}, and ν_1 at ~1086 cm^{-1}. In panel (d), the D and G bands are shown by blue and green vertical lines, respectively.

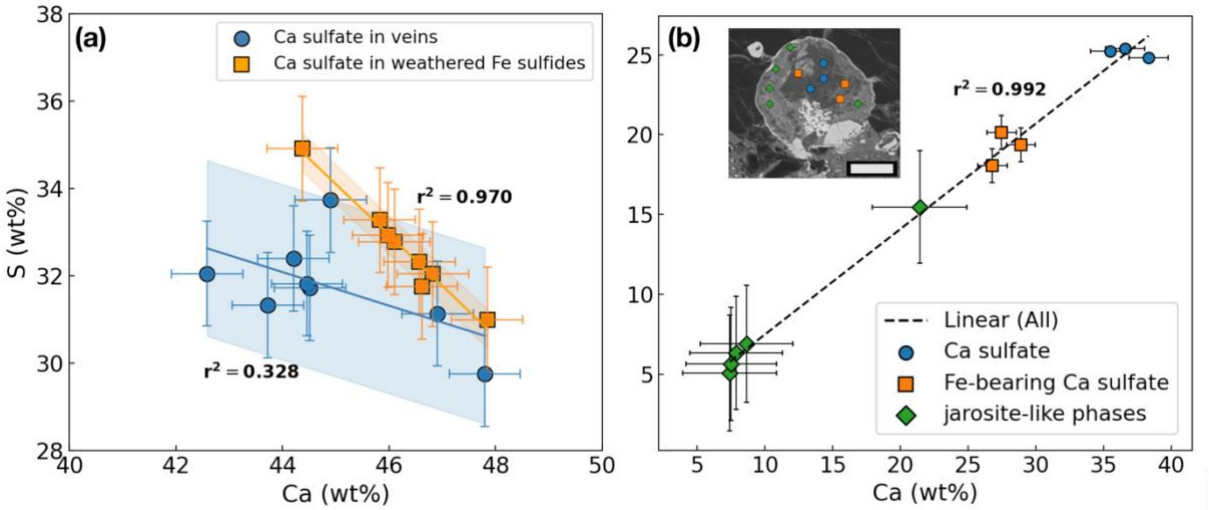

Fig. 8. Variation of Ca-S (wt%) in sulfate phases of LoV 123. (a) Semi-quantitative EDS point analyses of Ca sulfate in veins (blue) and Ca sulfate associated with weathered Fe sulfides (orange). Veins show no significant Ca-S correlation (r^2 = 0.328), whereas Ca sulfate replacing Fe sulfides displays a strong negative correlation (r^2=0.970). (b) Ca-S compositions of three phases within the sulfide-weathering products: Ca sulfate (blue circles), Fe-bearing Ca sulfate (orange squares), and jarosite-like phases (green diamonds). A single linear fit through all analyses is consistent with sub-micron intergrowths of these mineral phases. The BSE image of a weathered Fe sulfides nodule displays the EDS spot locations. Scale bar 20 μm.

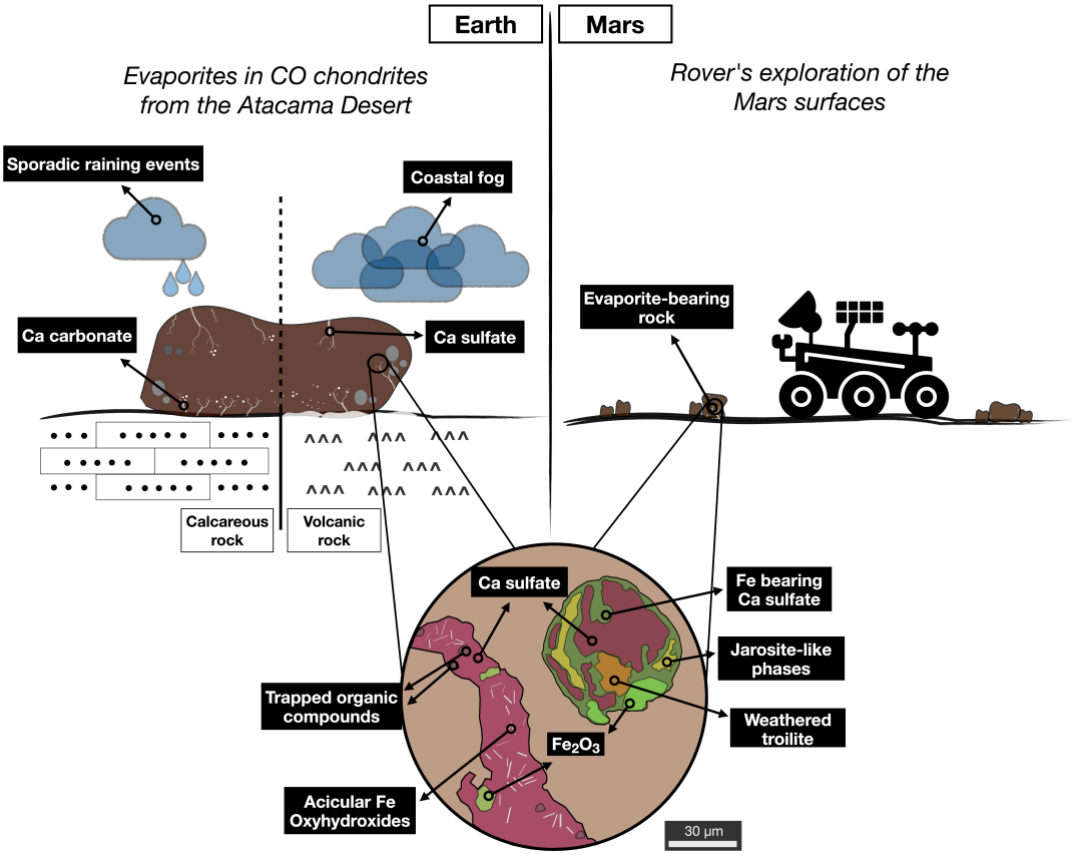

Fig. 9. Schematic representation of the proposed link between evaporites in Atacama CO chondrites and evaporite-bearing rock on Mars. Earth (left): Hyperarid Atacama settings where post-fall evaporites form in CO chondrites. Carbonates preferentially develop over calcareous substrates with sporadic rainfall (Calama area), whereas Ca sulfates dominate in coastal areas influenced by Pacific fog and interaction with volcanic substrates. Mars (right): Rover reconnaissance of evaporite-bearing outcrops. Simplified thin-section (center): view of CO chondrites showing typical associations of Ca sulfate (anhydrite-rich), Fe-bearing Ca sulfate, jarosite-like phase, goethite/hematite/Fe oxyhydroxides in weathered Fe sulfides and organic compounds trapped within sulfate microcavities on secondary veins. These evaporitic assemblages in Atacama CO chondrites provide a terrestrial analogue, at the process level, indicating anhydrite dominance under low water activity and localized retention of organic matter within sulfate phases.

References

Abreu, N. M., & Brearley, A. J. (2005). Carbonates in Vigarano: Terrestrial, preterrestrial, or both? Meteoritics & Planetary Science, 40(4), 695–708. https://doi.org/10.1111/j.1945-5100.2005.tb00966.x

Airieau, S. A., Farquhar, J., Thiemens, M. H., Leshin, L. A., Bao, H., & Young, E. (2005). Planetesimal sulfate and aqueous alteration in CM and CI carbonaceous chondrites. *Geochimica et Cosmochimica Acta, 69(16),* 4167-4172. https://doi.org/10.1016/j.gca.2005.01.029

Al Disi, Z. A., Sadooni, F., Al-Kuwari, H. A. S., & Bontognali, T. R. (2023). Microbially influenced formation of anhydrite at low temperature. *Science of the Total Environment*, *902*, 165820.

Alexander, C. O. D., Bowden, R., Fogel, M. L., & Howard, K. T. (2015). Carbonate abundances and isotopic compositions in chondrites. *Meteoritics & Planetary Science, 50(4),* 810-833.

Alexander, C. M. O. D., McKeegan, K. D., & Altwegg, K. (2018). Water reservoirs in small planetary bodies: meteorites, asteroids, and comets. *Space science reviews, 214(1),* 36.

Alvarez, J., Jorquera, R., Miralles, C., Padel, M., & Martínez, P. (2016). Cartas Punta Posallaves y Sierra Vicuña Mackenna, Región de Antofagasta. Servicio Nacional de Geología y Minería, Carta Geológica de Chile, Serie Geológica Básica No. 183-184. Región de Antofagasta, 147 p. Santiago.

Aref, M. A., & Taj, R. J. (2018). Recent evaporite deposition associated with microbial mats, Al-Kharrar supratidal–intertidal sabkha, Rabigh area, Red Sea coastal plain of Saudi Arabia. *Facies, 64(4),* 28.

Arens, F. L., Airo, A., Feige, J., Sager, C., Wiechert, U., & Schulze-Makuch, D. (2021). Geochemical proxies for water-soil interactions in the hyperarid Atacama Desert, Chile. *Catena, 206,* 105531.

Azimi, G., & Papangelakis, V. G. (2011). Mechanism and kinetics of gypsum–anhydrite transformation in aqueous electrolyte solutions. *Hydrometallurgy*, 108(1–2), 122–129.

Azua-Bustos, A., González-Silva, C., & Fairen, A. G. (2022). The Atacama Desert in northern Chile as an analog model of Mars. *Frontiers in Astronomy and Space Sciences, 8*, 810426.

Bao, H., Thiemens, M. H., Farquhar, J., Campbell, D. A., Lee, C. C.-W., Heine, K., & Loope, D. B. (2000). Anomalous ^{17}O compositions in massive sulphate deposits on the Earth. *Nature*, *406(6792),* 176–178.

Barrat, J. A., Gillet, P., Lecuyer, C., Sheppard, S. M. F., & Lesourd, M. (1998). Formation of carbonates in the Tatahouine meteorite. *Science, 280(5362),* 412-414.

Benzerara, K., Chapon, V., Moreira, D., López-García, P., Guyot, F., & Heulin, T. (2006). Microbial diversity on the Tatahouine meteorite. *Meteoritics & Planetary Science*, *41*(8), 1249-1265.

Bladh, K. W. (1982). The formation of goethite, jarosite, and alunite during the weathering of sulfide-bearing felsic rocks. *Economic Geology, 77(1*), 176-184.

Bland, P. A., Zolensky, M. E., Benedix, G. K., and Sephton, M. A. (2006). Weathering of Chondritic Meteorites. *In Meteorites and the Early Solar System II*, edited by D. S. Lauretta, and H. Y. McSween, 853–867. Tucson, AZ: University of Arizona Press.

Bonal, L., Quirico, E., Bourot-Denise, M., & Montagnac, G. (2006). Determination of the petrologic type of CV3 chondrites by Raman spectroscopy of included organic matter. *Geochimica et Cosmochimica Acta, 70(7),* 1849-1863.

Bonal, L., Quirico, E., Flandinet, L., & Montagnac, G. (2016). Thermal history of type 3 chondrites from the Antarctic meteorite collection determined by Raman spectroscopy of their polyaromatic carbonaceous matter. *Geochimica et Cosmochimica Acta, 189*, 312-337.

Busemann, H., Alexander, M. O. D., & Nittler, L. R. (2007). Characterization of insoluble organic matter in primitive meteorites by microRaman spectroscopy. *Meteoritics & Planetary Science, 42(7-8),* 1387-1416.

Butler, G.P., Harris, P.M., Kendall, C.G.S.T.C., (1982). Recent evaporites from the Abu Dhabi coastal flats. In: In: Handford, C.R., Loucks, R.G., Davies, G.R. (Eds.), *Depositional and Diagenetic Spectra of Evaporites 3*. pp. 33–64 SEPM core workshop.

Carter, J., Poulet, F., Bibring, J.-P., & Murchie, S. (2013). Hydrous minerals on Mars as seen by the CRISM and OMEGA imaging spectrometers: Updated global view. *Journal of Geophysical Research: Planets, 118(4),* 831–858.

Chan, Q. H. S., Zolensky, M. E., Bodnar, R. J., Farley, C., & Cheung J. C. H. (2017). Investigation of organo-carbonate associations in carbonaceous chondrites by Raman spectroscopy. *Geochimica et Cosmochimica Acta, 201*, 392–409. https://doi.org/10.1016/j.gca.2016.10.048

Charola, A. E., Pühringer, J., & Steiger, M. (2007). Gypsum: a review of its role in the deterioration of building materials. *Environmental geology, 52(2),* 339-352.

Chizmadia, L. J., Rubin, A. E., & Wasson, J. T. (2002). Mineralogy and petrology of amoeboid olivine inclusions in CO3 chondrites: Relationship to parent-body aqueous alteration. *Meteoritics & Planetary Science*, *37*(12), 1781-1796.

Cloots, R. (1991). Raman spectrum of carbonates MIICO3 in the 1100–1000 cm^{-1} region. *Spectrochimica Acta Part A: Molecular Spectroscopy, 47(10),* 1365–1369. https://doi.org/10.1016/0584-8539(91)80012-8

de Leuw, S., Rubin, A. E., & Wasson, J. T. (2010). Carbonates in CM chondrites: Complex formational histories. *Meteoritics & Planetary Science, 45(4),* 513–530.

de Wet, C. B., Godfrey, L., & de Wet, A. P. (2015). Sedimentology and stable isotopes from a lacustrine-to-palustrine limestone deposited in an arid setting, climatic and tectonic factors: Miocene–Pliocene Opache Formation, Atacama Desert, Chile. *Palaeogeography, Palaeoclimatology, Palaeoecology, 426*, 46-67.

Doyle, P. M., Jogo, K., Nagashima, K., Krot, A. N., Wakita, S., Ciesla, F. J., & Hutcheon, I. D. (2015). Early aqueous activity on the ordinary and carbonaceous chondrite parent bodies recorded by fayalite. *Nature Communications, 6(1),* 7444.

Drouard, A., Gattacceca, J., Hutzler, A., Rochette, P., Braucher, R., Bourlès, D., the ASTER Team, Gounelle, M., Morbidelli, A., Debaille, V., Van Ginneken, M., Valenzuela, M., Quesnel, Y., & Martinez, R. (2019). The meteorite flux of the past 2 m.y. recorded in the Atacama Desert. *Geology*, 47(7), 673–676.

Dutka, F., Starchenko, V., Osselin, F., Magni, S., Szymczak, P., & Ladd, A. J. (2020). Time-dependent shapes of a dissolving mineral grain: Comparisons of simulations with microfluidic experiments. *Chemical Geology, 540*, 119459.

Ebel, D. S., Brunner, C., Konrad, K., Leftwich, K., Erb, I., Lu, M., Rodriguez, H., Crapster-Pregont, E. J., Friedrich, J. M., & Weisberg, M. K. (2016). Abundance, major element composition and size of components and matrix in CV, CO and Acfer 094 chondrites. *Geochimica et Cosmochimica Acta, 172,* 322-356.

Ericksen, G. E. 1981. Geology and Origin of the Chilean Nitrate Deposits. *US Geological Survey, Professional Paper* 1188: 37.

Espinoza G., Felipe, Matthews, Stephen J., Cornejo P., Paula. (2012). Carta Los Vientos, Región de Antofagasta. Servicio Nacional de Geología y Minería, Carta Geológica de Chile, Serie Geológica Básica No. 138. Región de Antofagasta, 72 p. Santiago.

Fan, C., & Teng, H. H. (2007). Surface behavior of gypsum during dissolution in undersaturated conditions. *Geochimica et Cosmochimica Acta, 71(15),* 3796–3811.

Fredriksson K. and Kerridge J. F. (1988) Carbonates and sulfates in CI chondrites: Formation by aqueous activity on the parent body. *Meteoritics 23*, 35–44.

Gattacceca, J., McCubbin, F. M., Bouvier, A., & Grossman, J. N. (2020). The meteoritical bulletin, no. 108. *Meteoritics & Planetary Science*, *55*(5), 1146-1150.

González-Pinilla, F. J., Latorre, C., Rojas, M., Houston, J., Rocuant, M. I., Maldonado, A., Santoro, C. M., Quade, J., & Betancourt, J. L. (2021). High-and low-latitude forcings drive Atacama Desert rainfall variations over the past 16,000 years. *Science advances, 7(38),* eabg1333.

Goudie, A. S., Wright, E., and Viles, H. A. (2002). The Roles of Salt (Sodium Nitrate) and Fog in Weathering: A Laboratory Simulation of Conditions in the Northern Atacama Desert, Chile. *Catena 48:* 255–266.

Gounelle, M., & Zolensky, M. E. (2001). A terrestrial origin for sulfate veins in CI1 chondrites. *Meteoritics & Planetary Science, 36(10)*, 1321–1329.

Grady, M. M., & Wright, I. P. (2003). Elemental and isotopic abundances of carbon and nitrogen in meteorites. *Space Science Reviews*, *106(1),* 231-248.

Haenecour, P., Floss, C., Brearley, A. J., & Zega, T. J. (2020). The effects of secondary processing in the unique carbonaceous chondrite Miller Range 07687. *Meteoritics & Planetary Science*, 55(6), 1228-1256.

Haenecour, P., Floss, C., Zega, T. J., Croat, T. K., Wang, A., Jolliff, B. L., & Carpenter, P. (2018). Presolar silicates in the matrix and fine-grained rims around chondrules in primitive CO3.0 chondrites: Evidence for pre-accretionary aqueous alteration of the rims in the solar nebula. *Geochimica et Cosmochimica Acta*, 221, 379-405.

Hartley, A. J., & Chong, G. (2002). Late Pliocene age for the Atacama Desert: implications for the desertification of western South America. *Geology, 30(1),* 43-46.

Harvie, C. E., Weare, J. H., Hardie, L. A., & Eugster, H. P. (1980). Evaporation of seawater: calculated mineral sequences. *Science*, *208*(4443), 498-500.

Hanesch, M. (2009). Raman spectroscopy of iron oxides and (oxy)hydroxides at low laser power and possible applications in environmental magnetic studies. *Geophysical Journal International, 177(3),* 941–948. https://doi.org/10.1111/j.1365-246X.2009.04122.x

Huang, W., Ertekin, E., Wang, T., Cruz, L., Dailey, M., DiRuggiero, J., & Kisailus, D. (2020). Mechanism of water extraction from gypsum rock by desert colonizing microorganisms.

Proceedings of the National Academy of Sciences, 117(20), 10681–10687. https://doi.org/10.1073/pnas.2001613117

Hurowitz, J. A., Tice, M. M., Allwood, A. C., Cable, M. L., Hand, K. P., Murphy, A. E., ... & Wolf, Z. U. (2025). Redox-driven mineral and organic associations in Jezero Crater, Mars. *Nature, 645(8080)*, 332-340.

Huss G.R., Rubin A.E., & Grossman J.N. (2006) Thermal metamorphism in chondrites. In: Lauretta D, McSween HY Jr (eds) *Meteorites and the early solar system II*. Arizona University Press, Tucson, pp 567–586.

Hutzler, A., Gattacceca, J., Rochette, P., Braucher, R., Carro, B., Christensen, E. J., Cournede, C., et al. (2016). Description of a Very Dense Meteorite Collection Area in Western Atacama: Insight into the Long-Term Composition of the Meteorite Flux to Earth. *Meteoritics & Planetary Science 51*: 468–482.

Jenkins, L. E., Lee, M. R., Daly, L., King, A. J., Floyd, C. J., Martin, P. E., .Almeida, N., & Genge, M. J. (2024). Winchcombe: An example of rapid terrestrial alteration of a CM chondrite. *Meteoritics & Planetary Science, 59(5),* 988-1005. https://doi.org/10.1111/maps.13949

Kaskes P., Déhais T., de Graaff S.J., Goderis S. and Claeys P. (2021) Micro-X-ray fluorescence (μXRF) analysis of proximal impactites: High-resolution element mapping, digital image analysis, and quantifications. Large Meteorite Impacts and Planetary Evolution VI. Geological Society of America

Kuebler, K. E., Jolliff, B. L., Wang, A., & Haskin, L. A. (2006). Extracting olivine (Fo–Fa) compositions from Raman spectral peak positions. *Geochimica et Cosmochimica Acta, 70(24),* 6201–6222.

Klipsch, S., Voigt, C., Herwartz, D., Chong, G., & Staubwasser, M. (2023). Sulfate sources, biologic cycling, and mobility in Atacama Desert soils constrained by triple oxygen isotopes. *Global and Planetary Change, 229*, 104255.

King, A. J., Phillips, K. J. H., Strekopytov, S., Vita-Finzi, C., & Russell, S. S. (2020). Terrestrial modification of the Ivuna meteorite and a reassessment of the chemical composition of the CI type specimen. *Geochimica et Cosmochimica Acta, 268*, 73-89

Klingelhöfer, G., Bernhardt, B., Schröder, C., et al. (2004). Jarosite and hematite at Meridiani Planum from Opportunity's Mössbauer spectrometer. *Science, 306(5702),* 1740–1745. https://doi.org/10.1126/science.1104653

Krot, A. N., Petaev, M. I., Piani, L., Marrocchi, Y., Fujiya, W., Pravdivtseva, O. V., ... & Huss, G. R. (2025). Metasomatic alteration of type 3 ordinary and carbonaceous chondrites. *Space Science Reviews*, *221*(1), 7.

Kryachko, T., (2018) Photograph of meteorite (ID: 70592). Encyclopedia of Meteorites. Available at: https://encyclopedia-of-meteorites.com/Meteorite?id=70592 (accessed March 16, 2026).

Kurosawa, K., Ono, H., Niihara, T., Sakaiya, T., Kondo, T., Tomioka, N., ... & Matsui, T. (2022). Shock recovery with decaying compressive pulses: Shock effects in calcite (CaCO3) around the Hugoniot elastic limit. *Journal of Geophysical Research: Planets*, *127*(6), e2021JE007133.

Larrain, H., Velásquez, F., Cereceda, P., Espejo, R., Pinto, R., Osses, P., & Schemenauer, R. S. (2002). Fog measurements at the site "Falda Verde" north of Chañaral compared with other fog stations of Chile. *Atmospheric Research, 64(1-4)*, 273-284.

Lee, M. R. (1993). The petrography, mineralogy and origins of calcium sulphate within the Cold Bokkeveld CM carbonaceous chondrite. *Meteoritics*, 28(1), 53–62. https://doi.org/10.1111/j.1945-5100.1993.tb00248.x

Lee, M. R., & Bland, P. A. (2004). Mechanisms of weathering of meteorites recovered from hot and cold deserts and the formation of phyllosilicates. *Geochimica et Cosmochimica Acta*, *68*(4), 893-916.

Lee, M. R., Daly, L., Floyd, C., & Martin, P. E. (2021). CM carbonaceous chondrite falls and their terrestrial alteration. *Meteoritics & Planetary Science*, *56*(1), 34-48.

Lennaerts, D. S. R. (2013). *Effect of sample history on dissolution rates of gypsum {010} surfaces* (Master's thesis, Wright State University). Wright State University. https://corescholar.libraries.wright.edu/etd_all/1130/

Li, X., Chen, Y., Tang, X., Gu, L., Yuan, J., Su, W., Tian, H., Luo, H., Cai, S., & Komarneni, S. (2023). Thermally induced phase transition of troilite during Micro-Raman spectroscopy analysis. *Icarus*, *390*, 115299.

Lindstrom M. M. (1989). News and information. *Antarctic Meteorite Newsletter*, 12, no. 1:3.

Lobos-Roco, F., Suárez, F., Aguirre-Correa, F., Keim, K., Aguirre, I., Vargas, C., Abarca, F., Ramírez, C., Escobar, R., Osses, P., & Del Río, C. (2024). Understanding inland fog and dew dynamics for assessing potential non-rainfall water use in the Atacama. *Journal of Arid Environments*, 221, 105125.

Losiak, A., & Velbel, M. A. (2011). Evaporite formation during weathering of Antarctic meteorites—A weathering census analysis based on the ANSMET database. *Meteoritics & Planetary Science, 46(3)*, 443-458.

MacPherson, G. J. (2014). Calcium–aluminum-rich inclusions in chondritic meteorites. In *Meteorites, Comets and Planets*, edited by A. M Davis, Treatise on Geochemistry, vol. 1 (edited by H. D. Holland and K. K. Turekian), 139–179. Oxford: Elsevier.

Marrocchi, Y., Bekaert, D. V., & Piani, L. (2018). Origin and abundance of water in carbonaceous asteroids. *Earth and Planetary Science Letters, 482*, 23-32.

Madden MEE, Bodnar RJ, Rimstidt JD (2004) Jarosite as an indicator of water-limited chemical weathering on Mars. *Nature 431*:821–823

McCoy, T. J. and Russell, S. S., with Zega, T. J., Thomas-Keprta, K. L., Singerling, S. A., Brenker, F. E., Timms, N. E., et al. (2025). An Evaporite Sequence from Ancient Brine Recorded in Bennu Samples. *Nature 637:* 1072–77

McKay, C. P., Molaro, J. L., & Marinova, M. M. (2009). High-frequency rock temperature data from hyper-arid desert environments in the Atacama and the Antarctic Dry Valleys and implications for rock weathering. *Geomorphology, 110(3-4),* 182-187.

Murchie, S. L., Mustard, J. F., Ehlmann, B. L., et al. (2009). A synthesis of Martian aqueous mineralogy after 1 Mars year of observations from the Mars Reconnaissance Orbiter. *Journal of Geophysical Research: Planets, 114*, E00D06. https://doi.org/10.1029/2009JE003342

Nishiizumi, K., Elmore, D., & Kubik, P. W. (1989). Update on terrestrial ages of Antarctic meteorites. *Earth and Planetary Science Letters*, *93*(3-4), 299-313.

Nittler, L. R., Alexander, C. M. D., Davidson, J., Riebe, M. E., Stroud, R. M., & Wang, J. (2018). High abundances of presolar grains and 15N-rich organic matter in CO3. 0 chondrite Dominion Range 08006. *Geochimica et Cosmochimica Acta*, *226*, 107-131.

Ossorio, M., Pérez, P., & López-Andrés, S. (2014). The gypsum–anhydrite paradox revisited. *Chemical Geology, 386,* 16–21.

Pearson, V. K., Sephton, M. A., Franchi, I. A., Gibson, J. M., & Gilmour, I. (2006). Carbon and nitrogen in carbonaceous chondrites: Elemental abundances and stable isotopic compositions. *Meteoritics & Planetary Science, 41(12),* 1899–1918.

Phillips, M. S., Viviano, C. E., Rogers, A. D., Larson, L., Tornabene, L., Trowbridge, A., Moersch, J.E., & McSween Jr, H. Y. (2025). Widespread ancient anorthosites in the lower crust of Mars. *Communications Earth & Environment*, 6:1026.

Pinto, G. A., Jacquet, E., Corgne, A., Olivares, F., Villeneuve, J., & Marrocchi, Y. (2024a). Deciphering recycling processes during solar system evolution from magnesium-rich relict olivine grains in type II chondrules. *Geochimica et Cosmochimica Acta, 364,* 65-78.

Pinto, G. A., Lezcano, M. Á., Sanchéz-García, L., Martínez, R., Parro, V., & Carrizo, D. (2025). Higher Microbial Biomass Accumulation on El Médano 464 Meteorite Compared with Adjacent Soils in the Atacama Desert. *Astrobiology*, *25*(2), 115-132.

Pinto, G. A., Marrocchi, Y., Jacquet, E., & Olivares, F. (2022). Formation of chondrule fine-grained rims from local nebular reservoirs. *Meteoritics & Planetary Science, 57(5),* 1004-1017.

Pinto, G. A., Marrocchi, Y., Morbidelli, A., Charnoz, S., Varela, M. E., Soto, K., Martínez, R., & Olivares, F. (2021). Constraints on planetesimal accretion inferred from particle-size distribution in CO chondrites. *The Astrophysical journal letters, 917(2),* L25.

Pinto, G. A., Tavernier, A., Gattacceca, J., Corgne, A., Valenzuela, M., Luais, B., Flores, L., Olivares, F., and Marrocchi, Y. (2024b). Dense Collection Areas and Terrestrial Alteration of Meteorites in the Atacama Desert. *Meteoritics & Planetary Science 59*: 351–367.

Prestgard, T., Bonal, L., Eschrig, J., Gattacceca, J., Sonzogni, C., & Beck, P. (2021). Miller Range 07687 and its place within the CM-CO clan. *Meteoritics & Planetary Science*, *56(9),* 1758-1783.

Prieto-Taboada, N., Gómez-Laserna, O., Martínez-Arkarazo, I., Olazabal, M. Á., & Madariaga, J. M. (2014). Raman spectra of the different phases in the CaSO4–H2O system. *Analytical Chemistry, 86(19)*, 10131–10137.

Pourkhorsandi, H., d'Orazio, M., Rochette, P., Valenzuela, M., Gattacceca, J., Mirnejad, H., Sutter, B., Hutzler, A., & Aboulahris, M. (2017). Modification of REE distribution of ordinary chondrites from Atacama (Chile) and Lut (Iran) hot deserts: Insights into the chemical weathering of meteorites. *Meteoritics & Planetary Science, 52(9)*, 1843-1858.

Rech, J. A., Currie, B. S., Michalski, G., & Cowan, A. M. (2006). Neogene climate change and uplift in the Atacama Desert, Chile. *Geology, 34(9),* 761-764.

Rech, J. A., Quade, J., & Hart, W. S. (2003). Isotopic evidence for the source of Ca and S in soil gypsum, anhydrite and calcite in the Atacama Desert, Chile. *Geochimica et Cosmochimica Acta, 67(4),* 575-586.

Riquelme, R., Hérail, G., Martinod, J., Charrier, R., & Darrozes, J. (2007). Late Cenozoic geomorphologic signal of Andean forearc deformation and tilting associated with the uplift and climate changes of the Southern Atacama Desert (26 S–28 S). *Geomorphology, 86(3-4),* 283-306.

Sadaka, C., Gattacceca, J., Gounelle, M., Roskosz, M., Lagain, A., Tartese, R., Bonal, L., Maurel, C., Martínez, R., & Valenzuela, M. (2025). Systematic meteorite collection in the Catalina Dense Collection area (Chile): Description and statistics. *Meteoritics & Planetary Science, 60(2),* 308-323.

Sarma, L. P., Prasad, P. S. R., & Ravikumar, N. (1998). Raman spectroscopic study of phase transitions in natural gypsum. *Journal of Raman Spectroscopy, 29(9),* 851–856. https://doi.org/10.1002/(SICI)1097-4555(199809)29:9<851::AID-JRS313>3.0.CO;2-S

Savarino, J., Lee, C. C., & Thiemens, M. H. (2000). Laboratory oxygen isotopic study of sulfur (IV) oxidation: Origin of the mass-independent oxygen isotopic anomaly in atmospheric sulfates and sulfate mineral deposits on Earth. *Journal of Geophysical Research: Atmospheres, 105*(D23), 29079-29088.

Schindelin, J., Arganda-Carreras, I., Frise, E., et al. (2012). Fiji: An open-source platform for biological-image analysis. *Nature Methods, 9(7),* 676–682. https://doi.org/10.1038/nmeth.2019

Scott, E. R., & Jones, R. H. (1990). Disentangling nebular and asteroidal features of C03 carbonaceous chondrite meteorites. *Geochimica et Cosmochimica Acta*, 54(9), 2485-2502.

Sephton, M. A. (2002). Organic compounds in carbonaceous meteorites. *Natural product reports*, *19*(3), 292-311.

Shi, E., Wang, A., Hvidsten, O., et al. (2022). γ-CaSO4 with abnormally high stability from a hyperarid region on Earth and from Mars. *Journal of Geophysical Research: Planets, 127(7)*, e2021JE007108. https://doi.org/10.1029/2021JE007108

Soto, K., Valenzuela, M., Corgne, A., Gattacceca, J., Pinto, G. A., Martínez, R., & Pizarro, J. P. (2025). Terrestrial Ages of CO3 Chondrites from the Atacama Desert, Chile. *87th Annual Meeting of the Meteoritical Society,* Abstract #5238.

Sun, X., Amelung, W., Klumpp, E., Walk, J., Mörchen, R., Böhm, C., Moradi, G., May, S. M., Tamburini, F., Wang, Y., & Bol, R. (2024). Fog controls biological cycling of soil phosphorus in the Coastal Cordillera of the Atacama Desert. *Global Change Biology, 30(1),* e17068.

Suttle, M. D., King, A. J., Ramkissoon, N. K., Bonato, E., Franchi, I. A., Malley, J., ... & Russell, S. S. (2022). Alteration conditions on the CM and CV parent bodies–Insights from hydrothermal experiments with the CO chondrite Kainsaz. *Geochimica et Cosmochimica Acta*, *318*, 83-111.

Tait, A. W., Wilson, S., Tomkins, A. G., Hamilton, J. L., Gagen, E. J., Holman, A. I., Grice, K., Preston, L. J., Paterson, D. J., & Southam, G. (2022). Preservation of terrestrial microorganisms and organics within alteration products of chondritic meteorites from the Nullarbor Plain, Australia. *Astrobiology, 22(4),* 399-415.

Tomlinson, A. J., Blanco, N., Dilles, J. H., Maksaev, V., & Ladino, M. (2018). Carta Calama, Región de Antofagasta. Servicio Nacional de Geología y Minería, Carta Geológica de Chile, Serie Geológica Básica No. 199. Región de Antofagasta, 345p. Santiago.

Tomeoka, K., & Itoh, D. (2004). Sodium-metasomatism in chondrules in CO3 chondrites: Relationship to parent body thermal metamorphism. *Meteoritics & Planetary Science, 39(8),* 1359-1373.

Tritschler, U., Van Driessche, A. E., Kempter, A., Kellermeier, M., & Cölfen, H. (2015). Controlling the selective formation of calcium sulfate polymorphs at room temperature. *Angewandte Chemie International Edition*, 54(13), 4083-4086.

Tuinstra, F., & Koenig, J. L. (1970a). Raman spectrum of graphite. *The Journal of Chemical Physics, 53(3),* 1126–1130.

Tuinstra, F., & Koenig, J. L. (1970). Characterization of graphite fiber surfaces with Raman spectroscopy. *Journal of Composite Materials, 4(4),* 492-499

Tosca, N. J., & McLennan, S. M. (2009). Experimental constraints on the evaporation of partially oxidized acid-sulfate waters at the Martian surface. *Geochimica et Cosmochimica Acta, 73(4)*, 1205–1222. https://doi.org/10.1016/j.gca.2008.11.015

Tosca, N. J., Knoll, A. H., & McLennan, S. M. (2008). Water activity and the challenge for life on early Mars. *Science, 320(5880),* 1204–1207. https://doi.org/10.1126/science.1155432

Valenzuela, E. M. (2011). *Procesos de Meteorización en Condritos Ordinarios del Desierto de Atacama, Norte de Chile: Nuevos Antecedentes sobre Meteorización de Material Extraterrestre en Ambientes Desiertico*s. PhD thesis. Santiago, Chile: Universidad de Chile.

Van Driessche, A. E. S., Kellermeier, M., Benning, L. G., & Gebauer, D. (2019). Calcium sulfate precipitation pathways in natural and engineered environments: The role of nucleation, growth and transformation. *Chemical Geology, 530*, 119274. https://doi.org/10.1016/j.chemgeo.2019.119274

Vaniman, D., Chipera, S., Rampe, E., Bristow, T., Blake, D., Meusburger, J., et al. (2024). Gypsum on Mars: A detailed view at gale crater. *Minerals, 14(8),* 815.

Vaniman, D. T., Martínez, G. M., Rampe, E. B., Bristow, T. F., Blake, D. F., Yen, A. S., et al. (2018). Gypsum, bassanite, and anhydrite at Gale crater, Mars. *American Mineralogist, 103(7),* 1011-1020.

Velbel, M. A. (1988). The distribution and significance of evaporite minerals in meteorites from hot deserts. *Meteoritics*, 23(2), 151–159.

Velbel, M. A. (2014). Terrestrial weathering of ordinary chondrites in nature and continuing during laboratory storage and processing: Review and implications for Hayabusa sample integrity. *Meteoritics & Planetary Science*, *49*(2), 154-171.

Voigt, C., Klipsch, S., Herwartz, D., Chong, G., & Staubwasser, M. (2020). The spatial distribution of soluble salts in surface soils of the Atacama Desert and their relationship to climate and geomorphology. *Global and Planetary Change, 184*, 103077. https://doi.org/10.1016/j.gloplacha.2019.103077

Wehmann, N., Lenting, C., & Jahn, S. (2023). Calcium sulfates in planetary surface environments. *Global and Planetary Change, 230*, 104257.

Wlotzka, F. (1993). A weathering scale for the ordinary chondrites. *Meteoritics, vol. 28, no. 3, volume 28, page 460-460*, *28*.

Zolotov, M. Y., & Shock, E. L. (2005). Formation of jarosite-bearing deposits through aqueous oxidation of pyrite at Meridiani Planum, Mars. *Geophysical Research Letters, 32(21),* L21203.

Zurfluh, F. J., Hofmann, B. A., Gnos, E., & Eggenberger, U. (2013). "Sweating meteorites"—Water-soluble salts and temperature variation in ordinary chondrites and soil from the hot desert of Oman. *Meteoritics & Planetary Science, 48(10),* 1958-1980.

Zurfluh, F. J., Hofmann, B. A., Gnos, E., Eggenberger, U., & Jull, A. T. (2016). Weathering of ordinary chondrites from Oman: Correlation of weathering parameters with 14C terrestrial ages and a refined weathering scale. *Meteoritics & Planetary Science, 51(9),* 1685-1700.